STAT3 signaling induced by IL-6 family cytokines modulates angiogenesis

Julian Rapp, Malte Jung[1], Rhena F.U. Klar[2], Julian Wolf[1], Jakob Arnold[1], Oliver Gorka[3,4,5], Olaf Groß[3,4,5], Clemens Lange[1,6], Hansjürgen Agostini[1], Günther Schlunck[1], Felicitas Bucher[1,*]

[1]Eye Center, Medical Center – University of Freiburg, Faculty of Medicine, University of Freiburg, Germany
[2]Department of Medicine I, Medical Center – University of Freiburg, Faculty of Medicine, University of Freiburg, Germany
[3]Institute of Neuropathology, Medical Center – University of Freiburg, Faculty of Medicine, University of Freiburg, Germany
[4]Signalling Research Centres BIOSS and CIBSS, University of Freiburg, Freiburg, Germany
[5]Center for Basics in NeuroModulation (NeuroModulBasics), Faculty of Medicine, University of Freiburg, Freiburg, Germany
[6]Ophtha-Lab, Department of Ophthalmology, St. Franziskus Hospital Muenster, Muenster, Germany

*Corresponding Author: r. Felicitas Bucher, M.D.

Klinik für Augenheilkunde, Killianstraße 5

79106 Freiburg

felicitas.bucher@uniklinik-freiburg.de

Keywords: Angiogenesis, Endothelial cell, STAT3, IL-6 family cytokines, Oncostatin M, Ciliary neurotrophic factor.

Summary statement

STAT3 represents an attractive yet complex target in angiogenesis with its effects strongly dependent on its phosphorylation status and simultaneous activity of other intracellular signaling pathways

Abstract

Aberrant angiogenesis is a hallmark of cardiovascular and retinal neovascular disease. The STAT3 pathway represents a potential pharmacological target for those diseases due to its impact on angiogenesis. Surprisingly some STAT3 activators including the IL6 cytokine member oncostatin M (OSM) enhance angiogenesis whereas others like ciliary neurotropic factor (CNTF) reduce it. This study aims to clarify those conflicting effects. In contrast to the antiangiogenic cytokine CNTF, the proangiogenic OSM was able to activate intracellular signaling pathways beyond STAT3 including ERK and AKT. These differences translated into transcriptomic and metabolic shifts. siRNA mediated STAT3 knockdown experiments showed a decrease in VEGF-induced endothelial migration and sprouting while enhancing OSMs proangiogenic drive and switching CNTF's antiangiogenic to a proangiogenic response. These effects correlated with a transcriptomic shift representing enhanced STAT1 and ERK activity following STAT3 knockdown including a compensatory prolonged pSTAT1 activity. In conclusion, the angiogenic effect of STAT3 seems to be determined by cytokine-induced STAT3 specificity and simultaneous activity of other intracellular signaling pathways while the STAT3 pathway, predominantly recognized for its proangiogenic phenotypes, reveals novel antiangiogenic potential.

Introduction

Angiogenesis is a complex process that is critical to physiologic development as well as disease progression. It plays a key role in macro- as well as microvascular diseases including arteriosclerosis (Camaré et al., 2017), stroke (Navaratna et al., 2009; Deveza et al., 2012) and diabetic retinopathy (Crawford et al., 2009). Moreover, tumors tend to stimulate angiogenesis to fuel their need of metabolites for uninhibited growth (Viallard and Larrivée, 2017). Targeting angiogenesis hence represents an important therapeutic approach. Understanding the underlying mechanisms of angiogenesis on a molecular level is crucial prerequisite for the basis for identifying novel therapeutic targets.

The Vascular endothelial growth factor (VEGF) is to date the most prominent cytokine to regulate angiogenic processes in disease (Melincovici et al., 2018). A deeper understanding of the pathomechanisms behind specific diseases including arteriosclerosis and retinal neovascular disease, however, has revealed that inflammatory processes also modulate angiogenesis (Dan-Brezis et al., 2019; Wolf and Ley, 2019). Among others, the interleukin 6 (IL-6) cytokine family plays a key role in mediating inflammatory responses and shows potential to modify inflammation-induced angiogenesis (Zhang et al., 2015; Jones and Jenkins, 2018).

The IL-6 cytokine family consists of multiple cytokines including IL-6, ciliary neurotrophic factor (CNTF) and Oncostatin M (OSM) to name the most prominent. They all bind to a similar receptor complex, share intracellular signaling pathways and ultimately down-stream targets (Heinrich et al., 2003). All IL-6 cytokines signal through the gp130-mediated recruitment of receptor-associated Janus kinases which lead to phosphorylation and therefore activation of Signal Transducer and Activator of Transcription (STAT) proteins especially STAT3 (Heinrich et al., 2003; Jones and Jenkins, 2018). STAT3 was often reported to promote tumor growth (Johnson et al., 2018; Hu et al., 2019) and angiogenesis (Jung et al., 2005). However, the effects of IL-6 family cytokines on angiogenesis are inconsistent despite their shared activation of the STAT3 signaling pathway (Vasse et al., 1999; Bucher et al., 2016; Bucher et al., 2020).

Recent studies on CNTF suggest an anti-angiogenic effect of CNTF-induced STAT3 signaling on vascular endothelial cells and retinal angiogenesis (Bucher et al., 2016; Bucher et al., 2020). CNTF activates STAT3 by binding to a heterotrimeric receptor complex consisting of gp130, LIF-receptor beta (LIFRß) and the CNTF receptor α (CNTFRα). Interestingly, only few cell types including neurons and skeletal muscle cells express CNTFRα (Davis et al., 1991) but a soluble CNTFRα (sCNTFRα) enables other cell types including vascular endothelial cells to respond to CNTF signaling (Davis et al., 1993).

In contrast to CNTF, OSM elicits a pro-angiogenic response in vascular endothelial cells (Vasse et al., 1999), enhances tumor progression (Zhu et al., 2015) and is associated with cardiovascular disease (Modur et al., 1997; Abe et al., 2019). OSM-

induced intracellular signaling hence represents a potential target for new therapeutic approaches in neovascular disease (Kucia-Tran et al., 2018). Receptors necessary for OSM signaling, gp130 and OSMRβ, are widely distributed among different cell types (Richards, 2013) causing OSM to not only influence diseases related to angiogenic processes but also other diseases including bone remodeling, lung fibrosis or inflammatory skin conditions (Richards, 2013).

The reported inverse angio-modulatory effect of CNTF and OSM on vascular endothelial cells despite sharing STAT3 signaling as predominant intracellular signaling pathway, underlines that more research is needed to fully understand all aspects of cytokine-induced STAT3 signaling. Using *in vitro* angiogenesis models, we confirmed that OSM enhances vascular endothelial cell migration and sprouting whereas CNTF limits VEGF-induced endothelial sprouting. The degree of STAT3 specificity correlated with the angiogenic phenotype while STAT3 knock-down experiments suggested that the effect of STAT3 signaling on angiogenesis is highly context dependent and can result in pro- and antiangiogenic reactions. A detailed understanding of STAT3 activity in disease is therefore necessary to successfully use STAT3 as therapeutic target.

Results

OSM and CNTF have opposite angiomodulatory effects on vascular endothelial cells

To evaluate the effect of OSM and CNTF co-stimulated with its soluble CNTF-Rα (CNTF+R) on angiogenesis *in vitro*, both cytokines were tested in the spheroid-sprouting assay, the scratch wound assay and proliferation assay. OSM treatment provided a strong pro-angiogenic stimulus on vascular endothelial sprouting (OSM: Δ = +25%) compared to the basal sprouting rate (EBM control group). An additional pro-angiogenic impulse of 31% on top of VEGF-induced sprouting (VEGF control group) was induced after OSM+VEGF stimulation (Fig. 1A). In contrast, CNTF+R significantly reduced VEGF-initiated sprouting by 21.9% (Fig. 1A).

In the scratch wound assay, OSM treatment significantly enhanced endothelial migration after 10 h by 28.4% compared to EBM control (Fig. 1B). Interestingly,

OSM's pro-migratory stimulus surpassed the VEGF-induced effect within the first 10 h but stagnating afterwards while VEGF showed a consistent wound closing kinetic. In line with the observation in the spheroid sprouting assay, OSM in addition to VEGF significantly enhanced endothelial cell migration in comparison to VEGF alone by 29.3% after 10 h (Fig. 1B). In contrast, CNTF+R did not affect migration significantly with or without VEGF (Fig. 1B). Similar effects were seen with regards to cell proliferation: OSM significantly increased cell proliferation by 63.7% in contrast to EBM control and by 55.3% on top of VEGF-induced proliferation (Fig. 1C). CNTF+R again with or without VEGF was not able to achieve a significant effect on cell proliferation.

OSM, in contrast to CNTF+R, activates intracellular signaling pathways beyond STAT3

We hypothesized that the observed divergent effects of OSM and CNTF+R on endothelial cells correlated with distinct intracellular signaling patterns. Western blot analysis showed that OSM and CNTF+R both activated the STAT3 signaling pathway in HUVECs by phosphorylating the tyrosine 705 side (pSTAT3 Tyr 705) but only OSM was able to activate the Serine 727 (pSTAT3 Ser 727) side (Fig. 2A). STAT1 activation, as indicated by levels of pSTAT1 upon exposure to cytokines, was most prominent after OSM treatment while CNTF+R only led to a very weak pSTAT1 response (Fig. 2A). STAT5 activation was not prominent for both cytokines (Fig. 2A). Co-stimulation with VEGF led to the same results. (Fig. 2A). In contrast to CNTF+R, OSM also led to activation of other pathways including ERK and AKT represented by the increase in pERK and pAKT levels in response to OSM treatment (Fig. 2B) which was especially stable in the presence of VEGF (Fig. 2B).

To screen for an explanation of this different signaling patterns between OSM and CNTF+R, we further analyzed more upstream located proteins in the signaling cascade by measuring phosphorylation of Janus kinases (JAKs). Interestingly OSM and CNTF+R with or without VEGF co-stimulation did not generate a pJAK1 or pJAK2 signal in protein lysates after 5 min of stimulation but only OSM was able to introduce a statically significant pTYK2 activation (Supplemental Fig. S1A).

The time course of the intracellular signaling pathways revealed that both OSM as well as CNTF+R rapidly increased pSTAT3 levels, peaking at approximately 15 minutes with more prolonged activation by OSM (Supplemental Fig. S1B). ERK

signaling induced by OSM appeared more rapid and stronger, but of shorter duration than ERK activation induced by VEGF (Supplemental Fig. S1B). Interestingly the pSTAT3 Ser727 activation showed a slower activation pattern in contrast to the Y705 kinetics by peaking later at approximately 15 min (Supplemental Fig. S1B). This signaling kinetic aligned with the observed wound closure dynamic in OSM vs VEGF stimulated HUVECs. In summary, OSM activated multiple signaling pathways while CNTF+R showed STAT3 specificity with a minor activation of STAT1 (Fig. 2C).

OSM+VEGF and CNTF+R+VEGF induce a transcriptomic shift with many similarities but also distinct differences

Based on the observed differences in the angiomodulatory potential as well as intracellular signaling patterns between OSM and CNTF+R in the presence of VEGF, we next examined if these changes were associated with distinct gene expression profiles using RNA Seq analysis.

PCA of whole transcriptome sequencing data revealed that OSM+VEGF and CNTF+R+VEGF led to transcriptomic profiles clearly separating from the VEGF control group by the first principal component (PC1, Fig. 3A) while the second principal component separated biological replicates within the same group (PC2, Fig. 3A). In comparison to VEGF, only a small shift in the PC1 was observed between OSM+VEGF and CNTF+R+VEGF suggesting that the transcriptome of OSM+VEGF and CNTF+R+VEGF share many similarities in contrast to VEGF, but also distinct differences between each other. Comparing OSM+VEGF with the VEGF control group, 1392 DEGs were upregulated and 706 downregulated. Between CNTF+R+VEGF and the VEGF control group 1083 DEGs were upregulated and 431 downregulated. In contrast, only 92 genes were differentially upregulated and 35 differentially downregulated for OSM+VEGF in comparison to CNTF+R+VEGF (Fig. 3B). To identify genes responsible for the OSM-associated pro-angiogenic effect we compared the transcriptome of OSM+VEGF to CNTF+R+VEGF since the angiogenic differences should be reflected there. A GO-Term enrichment analysis of OSM+VEGF compared to CNTF+R+VEGF for biological processes identified “inflammatory response”, “response to cytokine” but also “cell migration” as part of the ten most enriched terms for OSM+VEGF (Fig. 3C). GO-Term enrichment analysis for molecular functions identified “cytokine receptor binding”, “growth factor binding” and “growth factor receptor binding” as one of the top enriched terms.

Besides those, GO-Term clusters associated with immunological processes were enriched which was also measurable in an enrichment analysis using the Reactome database resulting in enriched Interleukin signaling clusters for OSM+VEGF treated samples (Supplemental Fig. S2). Most of the DEGs annotated to the GO terms “cell migration”, “cytokine receptor binding”, “growth factor binding” and “growth factor receptor binding” showed strong fold changes and were highly significant for OSM+VEGF (Fig. 3D). Gene expression changes were consistent among biological replicates within the groups (Fig. 3E). Thus, the sequencing analysis suggests a conceivable role of the transcriptomic shifts inducing the observed angiogenic phenotype between OSM+VEGF and CNTF+R+VGEF treated samples.

STAT3 knock-down enhances OSM’s pro-angiogenic and inverts CNTF+Rs anti-angiogenic potential on HUVECs

Having established significant differences in angiogenic cell behavior in response to OSM compared to CNTF, we next assessed how the shared STAT3 pathway contributes to these phenotypes.

We established a STAT3 knock-down using siRNA which resulted in a potent knock-down persisting for up to 96 hours after transfection (Supplemental Fig. S3A). In the spheroid-sprouting assay, STAT3 knock-down abrogated the basal sprouting rate in the EBM group and decreased VEGF-induced sprouting by 39% compared to cells transfected with control siRNA (Fig. 4A). In contrast, STAT3 knock-down led to the opposite effect in OSM+VEGF stimulated HUVECs characterized by a 2.06-fold increase in sprouting compared to respective control siRNA transfected cells and a 4.7-fold increase compared to STAT3 knock-down cells treated with just VEGF.

STAT3 knockdown in HUVECs abolished CNTF+R’s ability to reduce VEGF-induced sprouting significantly and even increased endothelial sprouting in the CNTF+R+VEGF group compared to the VEGF group following STAT3 knock-down by a 1.78-fold change. HUVECs transfected with control siRNA and CNTF+R+VEGF treatment still reduced sprouting by 40.8% (Fig. 4A). Comparing CNTF+R+VEGF treated HUVECs with or without STAT3 knock-down, only a small difference was measurable despite the massive decrease in sprouting caused by the STAT3 knock-down in just VEGF treated samples (Fig. 4A).

Similar changes in response to STAT3 knock-down could be observed in the scratch wound assay. STAT3 knock-down reduced the wound closing kinetics of HUVECs in the EBM groups by 27.6% and in VEGF-treated group by 32.3% compared to the respective control siRNA treated cells after 14 h (Fig. 4B). Stimulation with OSM in STAT3 knock-down cells led to a strong increase by a 3.258-fold change compared to EBM stimulated knock-down cells (Fig. 4B). Comparable effects were observed in the presence of VEGF: co-stimulation with OSM+VEGF following STAT3 knock-down increased migration by 2.05-fold compared to VEGF after 14h (Fig. 4B). OSM treatment in control siRNA transfected cells still led to a 1.51-fold change increment of wound closing kinetics and co-stimulated with VEGF to 1.16-fold increment of wound closing kinetics. Surprisingly, STAT3 knock-down significantly decreased OSM+VEGF-induced cell proliferation (Supplemental Fig. S4) while VEGF induced proliferation was also significantly reduced, suggesting that the observed phenotype in the spheroid sprouting and migration assay are not based on enhanced proliferation but rather on migration and hypertrophy.

To ensure that the observed knock-down results were not skewed by siRNA off-target effects, we repeated selected knock-down experiments with a second STAT3 siRNA of a different sequence. STAT3 siRNA #2 resulted in a long lasting, efficient knock-down (Supplemental Fig. S3B). The spheroid-sprouting assay showed comparable changes in endothelial cell sprouting following STAT3 knock-down and OSM stimulation compared to STAT3 siRNA #1 (Supplemental Fig. S3C) validating our STAT3 knock-down data. The same tendencies for the second STAT3 siRNA were also measurable in a screening experiment for CNTF+R using the second STAT3 siRNA (Supplemental Fig. S3D).

To further validate the specificity of the observed STAT3-dependent phenotype, we established a STAT1 knock-down using siRNA (Supplemental Fig. S3E) and repeated the sprouting assay. Similar to the STAT3 knock-down, the STAT1 knock-down decreased the basal sprouting rate in every group (average decrease by -46.3%, Supplemental Fig. S3F). The increase in sprouting in the OSM treatment group was abolished following STAT1 knock-down. In contrast to the STAT3 knock-down that led to a significant increase in sprouting, OSM+VEGF only induced a weak increase in sprouting by 18.1% compared to VEGF following STAT1 knock-

down (Supplemental Fig. S3F). These data further validate the specificity of the observed STAT3-dependent knock-down data.

The increase in OSM's pro-angiogenic effect following STAT3 knock-down correlates with a shift in the balance of intracellular signaling pathways

To better understand the molecular mechanisms behind OSM's enhanced pro-angiogenic potential following STAT3 knockdown, we next performed an RNA sequencing analysis of HUVECs co-stimulated with OSM and VEGF following STAT3 knockdown (OMS+VEGF STAT3 siRNA) compared to control siRNA transfected cells (OSM+VEGF Control siRNA).

2410 DEGs were detected in the OSM+VEGF STAT3 siRNA group. GO enrichment analysis of all DEGs revealed many immunologic terms in line with the well-characterized role of STAT3 in inflammation. Interestingly, multiple GO terms associated with the regulation of the MAPK pathways and interferon gamma signaling pathway, which is closely connected to the STAT1 signaling pathway and known for its role in angiogenesis, were enriched as well (Fig. 5A). A pro-migrative transcriptome was also triggered by STAT3 knock-down in OSM+VEGF treated HUVECs indicated by the enrichment of the GO term "positive regulation of cell migration". Although knock-down cells showed a depletion of items associated with term of "negative regulation of growth" (Fig. 5A) as indicated by an enrichment in the control siRNA samples treated with OSM+VEGF in the RNA sequencing, this did not translate in a functional alteration as described earlier (Supplemental Fig. S4). Most of the DEGs annotated to GO terms associated with MAPK, cell migration and interferon-gamma activity presented good clustering on a sample-to-sample level (Fig. 5B). Three out of the 5 five most strongly expressed upregulated DEGs (Fig. 5C, marked in red) in OSM+VEGF treated STAT3 knockdown cells were part of the GO angiogenesis cluster (GO:0001525), which was not among the top 15 regulated GO terms shown in Figure 5A but also significantly enriched in knock-down cells. A GSEA confirmed that overall genes associated with the GO term angiogenesis were significantly enriched in the OSM+VEGF STAT3 siRNA group (Fig 5D). Taken together, these results strongly suggest that the enhanced pro-angiogenic effect of OSM in the absence of STAT3 relates to upregulation of STAT1- and ERK-dependent genes associated with cell proliferation and angiogenesis.

To understand, if a suspected compensatory upregulation of STAT1 and ERK signaling in response to STAT3 knock-down and OSM+VEGF treatment was specific to OSM, we also analyzed the transcriptomic profile of HUVECs treated with CNTF+R+VEGF following STAT3 knock-down (CNTF+R+VEGF STAT3 siRNA) as well as VEGF following STAT3 knockdown (VEGF STAT3 siRNA). Comparing CNTF+R+VEGF-treated knockdown and control transfected cells, multiple enriched GO terms associated with interferon gamma signaling but not MAPK signaling were identified (Supplemental Fig. 5A). These data align with initial analyses indicating that CNTF+R, in contrast to OSM, activated STAT3 and STAT1 signaling but not ERK (Fig. 2B). A Scatter plot of the data again illustrated many highly expressed DEGs annotated for GO angiogenesis including WARS1 and APLN (Supplemental Fig. 5B). GSEA also significantly enriched for the GO angiogenesis (Supplemental Fig. 5C). In contrast, VEGF stimulated HUVECs with or without STAT3 knock-down retrieved only 6 significantly enriched biological processes in the GO enrichment analysis (Supplemental Fig. 6A+B). Again, this aligns with the observation that VEGF does not induce STAT3 signaling in HUVECs.

The observed transcriptomic shifts in the OSM+VEGF as well as CNTF+R+VEGF treated groups following STAT3 knockdown point towards compensatory upregulation of STAT1 signaling and in case of OSM+VEGF ERK signaling. We therefore re-evaluated the activity of intracellular signaling pathways following STAT3 knock-down with cytokine stimulation on protein level using western blots. Following STAT3 knock-down and 5 min of OSM+VEGF stimulation there was no enhanced activation of pSTAT1, pSTAT5, pAKT and pERK while the pSTAT3 signal was clearly diminished (Fig. 6A). Time course experiments which screened for differences in pSTAT1 activity over 24 h, however, revealed that STAT3 knock-down cells showed a clearly prolonged pSTAT1 activity after 6 h and 24 h in response to OSM+VEGF treatment (Fig. 6B).

In summary, these data suggests that the extent of OSM's pro-angiogenic effect is tightly regulated by the balance of the intracellular signaling activity. Blocking STAT3 enhances cell migration and sprouting which is reflected by significantly upregulated genes associated with cell migration and compensatory signaling pathways including

ERK and AKT which in turn have been associated with a pro-angiogenic effect in the past. (Fig. 6C).

OSM shifts HUVECs to an active metabolic state by increasing mitochondrial performance

Examining alternative phosphorylation sides of STAT3 in response to OSM and CNTF, we observed that only OSM phosphorylated STAT3 not only at tyrosine 705, but also at the serine 727 side (pSTAT3Ser) (Fig. 2A).

pSTAT3Ser has been described to enhance STAT3's transcriptomic impact and furthermore modulate mitochondrial function and change consequently the metabolic rate of cells (Gough et al., 2009; Wegrzyn et al., 2009; Gough et al., 2014; Balic et al., 2020). We hypothesized that OSM increases the mitochondrial function of HUVECs by phosphorylation of STAT3 at the pSTAT3Ser side and thus provide energy and metabolites necessary for the enhanced angiogenic process. Using a system of OSM stimulated Bovine Aorta Endothelial Cells (BAECs) transfected with plasmids resulting in the expression of florescence tagged STAT3, a co-localization of STAT3 and stained mitochondria was evident (Fig. 7A). Unstimulated cells did not yield this result (Fig. 7A). Extracellular flux analysis of HUVECs pretreated with cytokines overnight for 15 hours provided a precise readout for further functional metabolic switches. Pretreatment with OSM or OSM+VEGF led to an increment of basal respiration, ATP production and maximal respiration in comparison to cells just treated with EBM (Fig. 7B, C). VEGF and CNTF+R did not significantly alter any of these functions.

To screen for potential molecular reasons that might explain the enhanced metabolic activity of HUVECs in response to OSM, we next studied levels of the mitochondrial respiratory chain complexes. Western blot analysis of all important complexes in the respiratory chain did not show any changes on protein level (Fig. 8A) or RNA level according to RNASeq (Supplemental Fig. S7). Major Production of superoxide was also not changed compared to control groups (Fig. 8B). While OSM induced mitochondrial activity consistently, its deeper molecular mechanisms remain to be elucidated.

OSM treatment enhances glycolysis

While measuring mitochondrial activity by extracellular flux analysis, OSM also revealed its ability to enhance glycolytic activity in vascular endothelial cells (Fig. 8C+D). This observation may be of particular relevance in the context of angiogenesis since glycolysis is believed to represent the main energy provider in hypoxia-driven aniogenic processes (Potente and Carmeliet, 2017). Quantification of the ECAR results revealed that baseline glycolytic activity was only significantly enhance in the VEGF+OSM group compared to VEGF while maximal glycolytic capacity was significantly increased in cells treated with OSM or OSM+VEGF compared to respective controls (Fig. 8C+D). In contract, CNTF+R stimulation did not result in similar changes (Fig. 8C+D).

Taken together, OSM's pro-angiogenic potential seems to be rooted in the activation of strong proliferative stimuli on a transcriptomic as well as metabolic level affecting mitochondrial respiration as well as glycolysis.

Discussion

In this study, we examined the angiomodulatory effects and underlying molecular changes of IL-6 family members and STAT3 activators OSM and CNTF to better characterize the role of STAT3 signaling in angiogenesis. Using *in vitro* angiogenesis assays we confirmed the previously described proangiogenic effect of OSM (Vasse et al., 1999) and antiangiogenic effect of CNTF (Bucher et al., 2016; Bucher et al., 2020) on vascular endothelial cells in standardized experimental settings (Fig. 1). Next, we were able to elucidate underlying mechanisms responsible for the inverse phenotype by characterizing intracellular signaling activity beyond STAT3 (Fig. 2). STAT3 knock-down experiments and RNA Seq analysis were used to further address the impact of STAT3 in the context of other proangiogenic signaling pathways (Fig. 4-6).

At first sight our results about the role of STAT3 signaling in vascular endothelial cells seem contradictory: a STAT3 knock-down decreased endothelial cell migration and sprouting in untreated, or VEGF stimulated cells, whereas a STAT3 knock-down

in IL-6 family cytokine-induced angiogenesis led to increased migration and sprouting (Fig. 4). Earlier studies on the role of STAT3 signaling in cell biology reveals that STAT3 modulates cellular functions on different levels depending on its subcellular localization and phosphorylation status (Avalle and Poli, 2018).

Our observation that STAT3 knock-down in unstimulated and VEGF-stimulated HUVECs significantly decreased endothelial cell migration and sprouting is in line with previously published data, which led to the common perception of STAT3 being a driver of angiogenesis (Jung et al., 2005; Johnson et al., 2018; Hu et al., 2019). Interestingly, both conditions (EBM as well as VEGF treatment) did not induce any baseline activation of the STAT3 signaling pathway represented by phosphorylation of STAT3 (Fig. 2). The measured decrease of angiogenesis might be due to a cytoplasmatic function of STAT3 independent of its phosphorylation status. Teng et. al. (Teng et al., 2009) proposed an interaction of STAT3 with the cytoskeleton which negatively affects cell migration after STAT3 loss. Ng, et al. (Ng et al., 2006) provided evidence for the interaction of STAT3 and the microtubule network showing that a STAT3 knock-down led to microtubule disassembly resulting in decreased endothelial capacity to migrate into a cell free area *in vitro*. Own immunohistochemical staining of the actin cytoskeleton by phalloidin suggested that STAT3 knock-down significantly reduced lamellipodia formation (data not shown) which is reported to be dependent on proper microtubule formation (Mikhailov and Gundersen, 1998). Furthermore, a role of unphosphorylated STAT3 as a transcription factor is also discussed in the literature (Timofeeva et al., 2012). This suggests that changes in expression levels of unphosphorylated STAT3 downstream targets could also be sufficient to induce shifts in phenotype due to STAT3 knock-down. While the idea of a protein-protein interaction of unphosphorylated STAT3 in the cytosol is still controversial, our own and previously published data suggest a more diverse role of STAT3 on cell biology beyond its role as transcription factor in its phosphorylated form.

Starting from the observed decrease in endothelial cell migration and sprouting in STAT3 knock-down cells following control and VEGF treatment, it was intriguing to observe an increase in endothelial cell migration and sprouting in response to OSM+VEGF or CNTF+R+VEGF stimulation following STAT3 knock-down (Fig. 4).

Treatment with OSM+VEGF or CNTF+R+VEGF had led to phosphorylation of STAT3 as well as other signaling molecules including ERK (Fig. 2) which was associated with distinct shifts in the transcriptomic profile (Fig. 3). Under the circumstance of STAT3 loss due to knock-down, other pathways in response to OSM+VEGF and CNTF+R+VEGF like pERK remained active (Fig. 6). We therefore assume that pSTAT3 balances the influence of pro-angiogenic drivers like ERK or AKT on a transcriptomic level. Besides clustering of ERK-associated GO terms, RNA Seq analysis in OSM+VEGF STAT3 siRNA cells showed enriched clusters of type I interferon and interferon-gamma associated signaling (Fig. 5A). We assume this is an indication for the increased impact of pSTAT1 on the transcriptome because type I interferon and interferon-gamme use the STAT1 pathway as a second messenger (Jung et al., 2021). Due to increased pSTAT1 impact on the transcriptome induced by the STAT3 knock-down both of those GO-terms enrich without any actual stimulation by type I interferons or interferon-gamma. Western blot analysis revealing prolonged pSTAT1 activity over 24 h after STAT3 knock-down support that hypothesis (Fig. 6B). Normally pSTAT1 activity is associated with an antiangiogenic probertites (Huang et al., 2002) which therefore questions the role of the prolonged pSTAT1 activity in the increased proangiogenic drive of OSM+VEGF after STAT3 knock-down. We assume therefore our data underline the important regulatory function of STAT3 on the activity of other signaling pathways which modulates their ability to change their capability of shifting the transcriptome which in total dictates the behavior of the endothelial cell.

The complexity of STAT3 signaling is further increased due to the existence of multiple phosphorylation sides which modulate STAT3 activity in different subcellular compartments. Besides the tyrosine 705 phosphorylation site STAT3 signaling can further be altered by phosphorylation at the serine 727 amino acid which is reported to increase mitochondrial performance and OXPHOS activity (Gough et al., 2009; Wegrzyn et al., 2009; Gough et al., 2014; Balic et al., 2020). In contrast to CNTF, only OSM led to STAT3 Ser727 phosphorylation (Fig. 2A). While vascular endothelial cells are known to mainly rely on glycolysis to fuel their need for ATP, they can also use mitochondrial oxidation under stress and as a biosynthetic hub to produce metabolites necessary for angiogenesis (Potente and Carmeliet, 2017). The molecular mechanism behind pSTAT3Ser's impact on cell metabolism is still not fully

understood. Current work suggests an interaction between STAT3 and complexes I and II to increase their activity leading to membrane potential enhancement (Wegrzyn et al., 2009) and a regulatory function in the production of reactive oxygen species (Gough et al., 2009). Mitochondrial STAT3 is also recognized to change mitochondrial gene expression (Carbognin et al., 2016). OSMs ability to increase mitochondrial performance and biogenesis while reducing apoptotic behavior has been reported in cardiomyocytes (Sun et al., 2015). Hanlon, et al. (Hanlon et al., 2019) recently described increased glycolysis in endothelial cells treated with OSM but no improvement in mitochondrial performance whereas our data suggest an increase in mitochondrial respiration as well as glycolysis (Fig. 7B+C, Fig. 8C+D). In contrast to our setup, Hanlon, et al. (Hanlon et al., 2019) pretreated HUVECs for 3h in comparison to our 15 h overnight incubation. The increase in OXPHOS might need more time to unfold while the boost in glycolysis measured by us Hanlon, et al. (Hanlon et al., 2019) represents a potentially immediate reaction. An instantaneously increased ECAR by an OSM injection on untreated cells in a Seahorse extracellular flux assay which we also measured (data not shown) supports this hypothesis. However, we did not observe OSM-associated differences by screening for major changes regarding expression levels of mitochondrial complexes or the production of reactive oxygen species induced by severe oxidative stress (Fig. 8A+B). The increased metabolic rate could be triggered by an unknown protein-protein interaction which warrants further understand the link between OSM and metabolism, especially because pSTAT3Ser induced metabolic switches were linked to disease progression (Zhang et al., 2013; Gough et al., 2014)

In summary, our study outlines the complex role of STAT3 signaling in vascular endothelial cells in response to cytokine treatment which consequently results in pleiotropic angiogenic effects. The angiomodulatory effect of STAT3 seems dependent on the activity of other intracellular signaling pathways as well as its subcellular localization in the cytosol, mitochondria or nucleus. OSM and CNTF differ in intracellular signaling patterns and their STAT3 specificity which translate into unique transcriptomic profiles and metabolic activity. A profound knowledge of these fine differences is necessary to understand the contribution of STAT3 signaling to disease progression and subsequently use STAT3 or STAT3-activating cytokines as therapeutic targets.

Materials and Methods

HUVEC Cell culture

Human Umbilical Vein Endothelial Cells (HUVECS, Human Umbilical Vein Endothelial Cells, Pooled, in EGM™-2, Cat#: C2519A, Lonza Group, Basel Switzerland) were grown in Endothelial Cell Growth Medium (EGM, Cat#: CC-3162, Lonza Group, Basel Switzerland) and used for all *in vitro* experiments.

For protein and RNA analyses, cells were stimulated by cytokines summarized in Table 1 which were diluted in endothelial cell growth basal medium (EBM-2 Endothelial Cell Growth Basal Medium-2, Cat#: CC-3156, Lonza Group, Basel Switzerland) supplemented with 6% fetal bovine serum (FBS, Cat#: S0615, Biochrome, Berlin, Germany). Cytokines and their concentrations can be found in the in the Supplemental Table S1. For protein analysis, cells were lysed after five minutes of cytokine stimulation using T-PER buffer (T-PER Tissue Protein Extraction Reagent, Cat#: 78510, Thermo Fisher Scientific, Waltham, MA, USA) supplemented with phosphatase and proteinase-inhibitor (Cat#: 87786 und 78420, Thermo Fisher Scientific, Waltham, MA, USA). For RNA sample generation, cells were lysed in QIAzol (QIAzol Lysis Reagent, Cat#: 79306, Qiagen, Hilden, Germany) 24 hours after stimulation.

Transfection

HUVECs were transfected using a loading solution of Opti-MEM (Opti-MEM™, Cat#: 31985062, Thermo Fisher Scientific, Waltham, MA, USA) containing 0.4% RNAiMAX (Lipofectamine™ RNAiMAX, Cat#: 137780309, Thermo Fisher Scientific, Waltham, MA, USA) and 15 nM STAT3 siRNA (STAT3 Stealth RNAi™ siRNA, Cat#: 1299001, siRNA ID: VHS40491 Thermo Fisher Scientific, Waltham, MA, USA), 120 nM STAT1 siRNA (STAT1 Stealth RNAi™ siRNA, Cat#: 1299001, siRNA ID: VHS40871, Thermo Fisher Scientific, Waltham, MA, USA) or control siRNA (Stealth RNAi™ siRNA negative control Med GC, Cat#: 12935300, Thermo Fisher Scientific, Waltham, MA, USA) for six hours. After six hours, wells were filled up to 2 mL using EGM. Cells were used for assays 48 hours after transfection. On target accuracy of the knock-down was evaluated by comparing effects of a second STAT3 siRNA (STAT3 Stealth RNAi™ siRNA, Cat#: 1299001, siRNA ID: VHS40497, Thermo Fisher Scientific, Waltham, MA, USA) with a completely different sequence.

SDS PAGE and Western blot

Protein samples were prepared for electrophoresis by denaturation using 75% sample, 22.5% Laemmli Buffer (4x Laemmli Sample Buffer, Cat#: 1610747, Bio-Rad Laboratories, Hercules, CA, USA) and 2.5% mercaptoethanol (2-Mercaptoethanol, Cat#: M3148, Sigma-Aldrich, Burlington, MA, USA). Samples were separated by SDS-PAGE and then transferred to a PVDF membrane (Immobilon-P PVDF Membrane, IPVH00010, Millipore, Burlington, MA, USA). Following a blocking step with 3% fetal bovine serum (BSA, Albumin, Rind, Fraktion V, Protease-free, Cat#: 11926.03, Serva, Heidelberg, Germany) for 30 minutes, membranes were stained with primary antibodies overnight at 4°C. Staining for GAPDH and secondary antibodies was conducted on the following day for one hour. All antibodies and their respective dilutions can be found in in in Supplemental Table S2. A Fusion FX system (Fusion FX, Vilber, Collégien, France) detected the signal using ECL (ECL™ Prime Western Blotting System, Cat#: RPN2232, GE Healthcare, Chicago, IL, USA). Figures show representative western blot results of 3 independent experiments. Where applicable, western blots were semiquantitative analyzed by using the b“ImageJ Fiji” software and its gel analyzer platform. Data was normalized on GAPDH expression for each lane which served as protein loading control. The relative fold of protein expression was finally calculated in percent by normalizing data on the specific control group. Uncut blots can be found in the supplemental material under ‘Blot transparency’ as Supplemental Figure S8-S12.

Spheroid Sprouting Assay

Spheroids formed in hanging drops of EGM containing 0.25% carboxy-methylcellulose (Methyl cellulose, Cat#: M0512, Sigma-Aldrich, Burlington, MA, USA) overnight were seeded in 0.5 mL of a collagen matrix consisting of 50% rat tail collagen (Collagen I, Rat Tail Cat#: 354236, Corning, Corning, NY, USA) and 48% EBM containing 0.25% carboxy-methylcellulose and 2% FBS. Collagen was titrated to a physiological pH by using sodium hydroxide (Sodium hydroxide, Cat#: P031.2, Roth, Karlsruhe, Germany) and buffered with 1 µL of a 1 M HEPES buffer (HEPES Buffer, Cat#: P05-01100, PAN Biotech, Aidenbach, Germany) After solidifying of the gel for 30 min, wells were layered with 100 µL EBM containing cytokines to match the desired final concentration. After incubation for one day, images of spheroids were taken using an inverse microscope (Zeiss Axio Vert. A1, Jena, Germany) and

the imaging software “ProgPres CapturePro 2.10.0.1” (JENOTIK Optical Systems, Jena, Germany). Quantification of all sprouts in each image took place using the measuring tool of “ImageJ Fiji”. The Relative Sprouting Length (RSL) per spheroid was used as a final readout by calculating the average cummulated sprouting length per spheroid normalized to a respective control in the same experiment.

Scratch Wound Assay

Migratory potential of HUVECs was measured by a standard scratch assay. 20000 HUVECs per well were seeded in EGM in IncuCyte ImageLock 96-well plates (IncuCyte® ImageLock 96-well Plates, Cat#: 4379, Sartorius, Göttingen, Germany) and starved overnight using EBM supplemented by 2% FBS and antibiotics. On the following day the scratch was created using the IncuCyte WoundMaker (IncuCyte® Cell Migration Kit, Cat#: 4493, Sartorius, Göttingen Germany) and wells were imaged every hour for 18 - 24 hours by the IncuCyte S3 Live-Cell Analysis System (IncuCyte® S3 Live-Cell Analysis System, Cat#: 4647, Sartorius, Göttingen Germany). For analysis, the integrated IncuCyte software (Integrated Cell Migration analysis module, Cat#: 9600-00-12, Sartorius, Göttingen, Germany) primed for HUVECs automatically detected cells and migration. The Relative Wound Density (RWD) was calculated automatically by the software and used as a final readout by dividing the confluence inside the originally scratched area by the confluence outside this area.

Proliferation Assay

3000 HUVECs were seeded into 96-well plates in EBM with 6% FBS. After 3 hours cells were stimulated by cytokines diluted in EBM supplemented by 6% FBS for a total of 72 hours with media change containing fresh cytokines every 24 hours. Cell number was determined by following the CyQUANT™ Cell Proliferation Assay protocol (CyQUANT™ Cell Proliferation Assay, Cat#: C7026, Thermo Fisher Scientific, Waltham, MA, USA). The readout was normalized to the specific control group during data analysis.

Extracellular flux analysis

Metabolic shifts were assessed using extracellular flux analysis by a Seahorse XFe96 Analyzer (Agilent Technologies, Santa Clara, CA, USA) measuring oxygen

consumption rate (OCR) and extracellular acidification rate (ECAR). 20000 cells were seeded in 96-well Seahorse cell culture plates (Seahorse XF96 V3 PS Cell Culture Microplates, Cat#: 101085-004, Agilent Technologies, Santa Clara, CA, USA) and pretreated for 15 hours overnight with cytokines. Medium of cells was changed after one washing step one hour before the assay to plain DMEM (DMEM, Cat#: D5030, Sigma-Aldrich, Burlington, MA, USA) titrated to pH 7.4 and supplemented with 10 mM glucose (Seahorse XF 1.0 M glucose solution, Cat#: 103577-100, Agilent Technologies, Santa Clara, CA, USA), 2 mM glutamine (Seahorse XF 200 mM glutamine solution, Cat#: 103579-100, Agilent Technologies, Santa Clara, CA, USA) and 10 mM HEPES. A typical injection strategy for the mitochondrial stress test was performed by injecting oligomycin (Oligomycin, Cat#: 495455, Sigma-Aldrich, Burlington, MA, USA) first followed by carbonyl cyanide-p-trifluoromethoxyphenylhydrazone (FCCP, Cat#: C2920, Sigma-Aldrich, Burlington, MA, USA), finalized by antimycin A (Antimycin A, Cat#: A8674, Sigma-Aldrich, Burlington, MA, USA) and rotenone (Rotenone, Cat#: R8875, Sigma-Aldrich, Burlington, MA, USA). The final concentration for oligomycin was 20 µM, 1.25 µM for FCCP and 2 µM for antimycin A and rotenone. Gathered data was normalized on cell count in each well measured by CyQUANT™ Cell Proliferation Assay and the average of cells in the EBM control group wells as reference. The smallest measurement of OCR after the last injection defined the non-mitochondrial oxygen consumption. Baseline was determined by the lowest measurement of OCR before oligomycin injection subtracted from the non-mitochondrial oxygen consumption. ATP production related OCR was calculated by the difference between the baseline and the lowest measurement following oligomycin injection. Finally, the highest OCR after FCCP injection subtracted from non-mitochondrial oxygen consumption defined the maximal respiration.

Co-staining of STAT3 and mitochondria

Plasmids coding for Venus1 STAT3 (Venus2-WTSTAT3 (Letra-Vilela et al., 2020), Cat#: 123164, addgene, Watertown, USA) and Venus2 STAT3 (Venus2-WTSTAT3 (Letra-Vilela et al., 2020), Cat#: 123165, addgene, Watertown, USA) were purchased and transformed in bacteria following the One Shot™ Stbl3™ (One Shot™ Stbl3™, Cat#: C737303, Thermo Fisher Scientific, Waltham, MA, USA) protocols. 1mL of the generated stock solution was plated on agar plates and grown

overnight in the incubator. Plasmids were isolated using standard procedures of the Plasmid DNA Purification Mini Prep Kit (Plasmid DNA Purification Mini Prep Kit, Cat#: S5369.0050, GENAXXON bioscience, Ulm, Germany). For quality control, plasmids were digested using the enzymes BrsGI (BsrGI, Cat#: R0575S, New England BioLabs, Ipswich, MA, USA) and NotI (NotI, Cat#: R0189S, New England BioLabs, Ipswich, MA, USA) according to the protocol generated for these enzymes by NEBcloner (https://nebcloner.neb.com/#!/protocol/re/double/BsrGI,NotI), plasmid fragments amplified by standard PCR and DNA detected on a 1% agarose gel.

For transfection experiments, Bovine Aorta Endothelial Cells (BAECs, Cat#: GM-7373, Leibniz Institut - Deutsche Sammlung von Mikroorganismen und Zellkulturen, Leipzig, Germany) cultured on fibronectin-coated flasks (Human Plasma Fibronectin Purified Protein, Cat#: FC010, Merck, Darmstadt, Germany) were used. BAECs were transfected with Venus1 STAT3 (1,04ng/µl) and Venus2 STAT3 (1,04ng/µl) in 8,3% Lipofectamine (Lipofectamine™ 2000, Cat#: 11668030, Thermo Fisher Scientific, Waltham, MA, USA) containing medium. After 24 h cells were stimulated with cytokines for 30 min and fixed with 2% paraformaldehyde for 20 minutes and blocked with 10% goat serum (Normal Goat Serum, Cat#: 005-000-121, Jackson ImmunoReseach Laboratories, Ely, UK) for one hour. Cells were stained by Mitoracker Orange (MitoTracker™ Orange CMTMRos, Cat#: M7510, Thermo Fischer Scientific, Waltham, MA, USA) following its protocol using a 1:3000 dilution. A Leica TCS SP8 confocal microscope (Leica, Wetzlar, Germany) and LASX 3.5.7 software generated high quality representative images.

Mitochondrial Assays

ROS production following cytokine pretreatment over night was measured using MitoSOX (MitoSOX Red Mitochondrial Superoxide Indicator, Cat#: M36008, Thermo Fischer Scientific, Waltham, MA, USA). The signal was analyzed by a LSR Fortessa flow cytometer. Debris and duplets were excluded from the analysis by gating using the FlowJo v10 software (FlowJo LLC, Becton Dickinson, Franklin Lakes, NJ, USA).

RNA sequencing

RNA isolation and all steps necessary for total RNA sequencing was conducted by “KFB - Center of Excellence for Fluorescent Bioanalytics” (University of Regensburg, Germany; www.kfb-regensburg.de). Samples were lysed in QIazol and shipped on

dry ice. Whole RNA was isolated following the RNeasy Micro Kit (RNeasy Micro Kit, Cat#: 74004, Qiagen, Hilden Germany) including the on-column DNase digestion and homogenization by Precellys CK14 ceramic beads before extraction. A combination of the Illumina TruSeq Stranded mRNA Sample Preparation Guide (TruSeq Stranded mRNA, Cat#: 20020594, Illumina, San Diego, CA, USA) and the Illumina NextSeq 2000 Sequencing System was used for library preparation and processing samples. Equimolar amounts of each library quantified by KAPA Library Quantification (KAPA Library Quantification Kit (ABI Prism®), Cat#: KK4835, Roche Sequencing Solutions, Basel, Switzerland) were sequenced on a NextSeq 2000 instrument controlled by the NextSeq 2000 Control Software (NCS) v1.1.0.27334, using two 100 cycles P2 Flow Cells with the single index, single-read (SR) run parameters. Base calling and imaging analysis were done by the Real Time Analysis Software (RTA) v3.6.14. Resulting cbcl files were converted into fastq files with the bcl2fastq v2.20 software.

Bioinformatics

Raw data was uploaded to Galaxy.eu (https://usegalaxy.eu) for further analysis (Afgan et al., 2018). FastQC (Galaxy Version 0.72) (Andrews) provided quality assessment of all raw files and STAR aligner (Galaxy Version 2.7.5b) (Dobin et al., 2012) mapped all reads to a human reference genome provided by GENCODE (GRCh38, release date 03.2020). Aligned reads were assigned to specific genes by featureCounts (Galaxy Version 1.6.4) (Liao et al., 2013) using the annotation file provided by GENCODE for the same reference genome. For all tools standard settings were applied. Downstream analysis was performed in R 4.0.2 (https://www.r-project.org) by normalizing counts using the DESeq2 package (Love et al., 2014). Ensembl ID (version 101) was matched to HGNC gene abbreviations by biomaRt. Genes were considered differentially expressed genes (DEG) at strict thresholds of adjusted p value < 0.05 using the methods of Benjamini and Hochberg and an absolute log2-foldchange of > 1. Gene Ontology (GO) enrichment analysis was conducted by the clusterProfiler R package (Yu et al., 2012), pathway enrichment analysis using the Reactome database by ReactomePA (Yu and He, 2016) and GSEA by ranking for shrinked log2-foldchanges by fgsea (Sergushichev, 2016) and MSigDB genesets for GO terms (downloaded 8th of April 2021)

Statistics

Error bars show mean +/- standard error of the mean. Statistical testing was performed by a Mann-Whitney-Test or, when multiple samples were compared, by a Kruskal–Wallis Test adjusted for multiple testing using the methods described by Benjamini, Krieger and Yekutieli. P values < 0.05 were considered significant and marked with a asterisk. P values of < 0.01 were visualized by two asterisks and smaller value then 0.001 by three asterisks.

Acknowledgments

The authors thank, Patrick Metzger and Melanie Börries from the Institute of Medical Bioinformatics and Systems Medicine, Medical Center – University of Freiburg for advice concerning analysis of sequencing data. We would like to acknowledge the Lighthouse Core Facility, Medical Center – University of Freiburg for their assistance with the Migration Assay and the Kompetenzzentrum Fluoreszente Bioanalytik, Regensburg for sequencing services.

Competing interests

FB has the following potential conflicts of interest to declare: funding for scientific research projects from Roche and Neurotech pharmaceuticals. Speaker activity for Novartis and Bayer.

Funding

This work was supported by the Deutsche Forschungsgemeinschaft [Bu3135/3-1to F.B., CRC 850, project C09 to R.F.U., SFB 1160 to O.Gr, SFB/TRR 167 to O.Gr, SFB 1425 to O.Gr, SFB 1479 to O.Gr, GRK 2606 to O.Gr, CIBSS - EXC-2189 - Project ID 390939984 to O.Gr], the Retinologische Gesellschaft, Germany [Dr. Werner-Jackstädt-Nachwuchspreis to F.B.], the Medizinische Fakultät der Albert-Ludwigs-Universität Freiburg [Berta-Ottenstein-Program for Clinician Scientists and Advanced Clinician Scientists to F.B., MOTI-VATE Program to J.R.] and the European Research Council [337689 and 966687 to O.Gr]

Data availability statement

The datasets presented in this study can be found in online repositories. The names of the repositories and accession numbers can be found below:
https://www.ncbi.nlm.nih.gov/geo/, GSE196776
https://www.ncbi.nlm.nih.gov/geo/, GSE198484.

References

Abe, H., Takeda, N., Isagawa, T., Semba, H., Nishimura, S., Morioka, M.S., et al. (2019). Macrophage hypoxia signaling regulates cardiac fibrosis via Oncostatin M. *Nat Commun* 10(1)**,** 2824. doi: 10.1038/s41467-019-10859-w.

Afgan, E., Baker, D., Batut, B., van den Beek, M., Bouvier, D., Čech, M., et al. (2018). The Galaxy platform for accessible, reproducible and collaborative biomedical analyses: 2018 update. *Nucleic Acids Research* 46(W1)**,** W537-W544. doi: 10.1093/nar/gky379.

Andrews, S. "FastQC A Quality Control tool for High Throughput Sequence Data".).

Avalle, L., and Poli, V. (2018). Nucleus, Mitochondrion, or Reticulum? STAT3 à La Carte. *Int J Mol Sci* 19(9). doi: 10.3390/ijms19092820.

Balic, J.J., Albargy, H., Luu, K., Kirby, F.J., Jayasekara, W.S.N., Mansell, F., et al. (2020). STAT3 serine phosphorylation is required for TLR4 metabolic reprogramming and IL-1β expression. *Nature Communications* 11(1)**,** 3816. doi: 10.1038/s41467-020-17669-5.

Boulton, T.G., Stahl, N., and Yancopoulos, G.D. (1994). Ciliary neurotrophic factor/leukemia inhibitory factor/interleukin 6/oncostatin M family of cytokines induces tyrosine phosphorylation of a common set of proteins overlapping those induced by other cytokines and growth factors. *Journal of Biological Chemistry* 269(15)**,** 11648-11655.

Bucher, F., Aguilar, E., Marra, K.V., Rapp, J., Arnold, J., Diaz-Aguilar, S., et al. (2020). CNTF Prevents Development of Outer Retinal Neovascularization Through Upregulation of CxCl10. *Investigative ophthalmology & visual science* 61(10)**,** 20-20. doi: 10.1167/iovs.61.10.20.

Bucher, F., Walz, J.M., Bühler, A., Aguilar, E., Lange, C., Diaz-Aguilar, S., et al. (2016). CNTF Attenuates Vasoproliferative Changes Through Upregulation of SOCS3 in a Mouse-Model of Oxygen-Induced Retinopathy. *Investigative ophthalmology & visual science* 57(10), 4017-4026. doi: 10.1167/iovs.15-18508.

Camaré, C., Pucelle, M., Nègre-Salvayre, A., and Salvayre, R. (2017). Angiogenesis in the atherosclerotic plaque. *Redox Biol* 12, 18-34. doi: 10.1016/j.redox.2017.01.007.

Carbognin, E., Betto, R.M., Soriano, M.E., Smith, A.G., and Martello, G. (2016). Stat3 promotes mitochondrial transcription and oxidative respiration during maintenance and induction of naive pluripotency. *The EMBO journal* 35(6), 618-634.

Crawford, T.N., Alfaro, D.V., 3rd, Kerrison, J.B., and Jablon, E.P. (2009). Diabetic retinopathy and angiogenesis. *Curr Diabetes Rev* 5(1), 8-13. doi: 10.2174/157339909787314149.

Dan-Brezis, I., Zahavi, A., Axer-Siegel, R., Nisgav, Y., Dahbash, M., Weinberger, D., et al. (2019). Inflammation, angiogenesis and coagulation interplay in a variety of retinal diseases. *Acta Ophthalmol*. doi: 10.1111/aos.14331.

Davis, S., Aldrich, T.H., Ip, N.Y., Stahl, N., Scherer, S., Farruggella, T., et al. (1993). Released form of CNTF receptor alpha component as a soluble mediator of CNTF responses. *Science* 259(5102), 1736-1739. doi: 10.1126/science.7681218.

Davis, S., Aldrich, T.H., Valenzuela, D.M., Wong, V.V., Furth, M.E., Squinto, S.P., et al. (1991). The receptor for ciliary neurotrophic factor. *Science* 253(5015), 59-63. doi: 10.1126/science.1648265.

Deveza, L., Choi, J., and Yang, F. (2012). Therapeutic angiogenesis for treating cardiovascular diseases. *Theranostics* 2(8), 801-814. doi: 10.7150/thno.4419.

Dobin, A., Davis, C.A., Schlesinger, F., Drenkow, J., Zaleski, C., Jha, S., et al. (2012). STAR: ultrafast universal RNA-seq aligner. *Bioinformatics* 29(1), 15-21. doi: 10.1093/bioinformatics/bts635.

Gong, Z., Ma, J., Su, H., Guo, T., Cai, H., Chen, Q., et al. (2018). Interleukin-1 receptor antagonist inhibits angiogenesis in gastric cancer. *International journal of clinical oncology* 23(4), 659-670. doi: 10.1007/s10147-018-1242-2.

Gough, D.J., Corlett, A., Schlessinger, K., Wegrzyn, J., Larner, A.C., and Levy, D.E. (2009). Mitochondrial STAT3 supports Ras-dependent oncogenic transformation. *Science* 324(5935)**,** 1713-1716.

Gough, D.J., Marié, I.J., Lobry, C., Aifantis, I., and Levy, D.E. (2014). STAT3 supports experimental K-RasG12D–induced murine myeloproliferative neoplasms dependent on serine phosphorylation. *Blood, The Journal of the American Society of Hematology* 124(14)**,** 2252-2261.

Hanlon, M.M., Rakovich, T., Cunningham, C.C., Ansboro, S., Veale, D.J., Fearon, U., et al. (2019). STAT3 Mediates the Differential Effects of Oncostatin M and TNFα on RA Synovial Fibroblast and Endothelial Cell Function. *Frontiers in Immunology* 10(2056). doi: 10.3389/fimmu.2019.02056.

Hayashi, H., Sano, H., Seo, S., and Kume, T. (2008). The Foxc2 Transcription Factor Regulates Angiogenesis via Induction of Integrin β3 Expression*. *Journal of Biological Chemistry* 283(35)**,** 23791-23800. doi: https://doi.org/10.1074/jbc.M800190200.

Heinrich, P.C., Behrmann, I., Haan, S., Hermanns, H.M., Müller-Newen, G., and Schaper, F. (2003). Principles of interleukin (IL)-6-type cytokine signalling and its regulation. *Biochem J* 374(Pt 1)**,** 1-20. doi: 10.1042/bj20030407.

Hu, Y.S., Han, X., and Liu, X.H. (2019). STAT3: A Potential Drug Target for Tumor and Inflammation. *Curr Top Med Chem* 19(15)**,** 1305-1317. doi: 10.2174/1568026619666190620145052.

Huang, S., Bucana, C.D., Van Arsdall, M., and Fidler, I.J. (2002). Stat1 negatively regulates angiogenesis, tumorigenicity and metastasis of tumor cells. *Oncogene* 21(16)**,** 2504-2512. doi: 10.1038/sj.onc.1205341.

Johnson, D.E., O'Keefe, R.A., and Grandis, J.R. (2018). Targeting the IL-6/JAK/STAT3 signalling axis in cancer. *Nat Rev Clin Oncol* 15(4)**,** 234-248. doi: 10.1038/nrclinonc.2018.8.

Jones, S.A., and Jenkins, B.J. (2018). Recent insights into targeting the IL-6 cytokine family in inflammatory diseases and cancer. *Nature Reviews Immunology* 18(12)**,** 773-789. doi: 10.1038/s41577-018-0066-7.

Jung, I., Jung, D., Zha, Z., Jeong, J., Noh, S., Shin, J., et al. (2021). Interferon-γ inhibits retinal neovascularization in a mouse model of ischemic retinopathy. *Cytokine* 143**,** 155542. doi: 10.1016/j.cyto.2021.155542.

Jung, J.E., Lee, H.G., Cho, I.H., Chung, D.H., Yoon, S.H., Yang, Y.M., et al. (2005). STAT3 is a potential modulator of HIF-1-mediated VEGF expression in human renal carcinoma cells. *Faseb j* 19(10)**,** 1296-1298. doi: 10.1096/fj.04-3099fje.

Kucia-Tran, J.A., Tulkki, V., Scarpini, C.G., Smith, S., Wallberg, M., Paez-Ribes, M., et al. (2018). Anti-oncostatin M antibody inhibits the pro-malignant effects of oncostatin M receptor overexpression in squamous cell carcinoma. *The Journal of Pathology* 244(3)**,** 283-295. doi: https://doi.org/10.1002/path.5010.

Letra-Vilela, R., Cardoso, B., Silva-Almeida, C., Maia Rocha, A., Murtinheira, F., Branco-Santos, J., et al. (2020). Can asymmetric post-translational modifications regulate the behavior of STAT3 homodimers? *FASEB Bioadv* 2(2)**,** 116-125. doi: 10.1096/fba.2019-00049.

Liao, Y., Smyth, G.K., and Shi, W. (2013). featureCounts: an efficient general purpose program for assigning sequence reads to genomic features. *Bioinformatics* 30(7)**,** 923-930. doi: 10.1093/bioinformatics/btt656.

Love, M.I., Huber, W., and Anders, S. (2014). Moderated estimation of fold change and dispersion for RNA-seq data with DESeq2. *Genome Biology* 15(12)**,** 550. doi: 10.1186/s13059-014-0550-8.

Melincovici, C.S., Boşca, A.B., Şuşman, S., Mărginean, M., Mihu, C., Istrate, M., et al. (2018). Vascular endothelial growth factor (VEGF) - key factor in normal and pathological angiogenesis. *Rom J Morphol Embryol* 59(2)**,** 455-467.

Mikhailov, A., and Gundersen, G.G. (1998). Relationship between microtubule dynamics and lamellipodium formation revealed by direct imaging of microtubules in cells treated with nocodazole or taxol. *Cell Motil Cytoskeleton* 41(4)**,** 325-340. doi: 10.1002/(sici)1097-0169(1998)41:4<325::Aid-cm5>3.0.Co;2-d.

Modur, V., Feldhaus, M.J., Weyrich, A.S., Jicha, D.L., Prescott, S.M., Zimmerman, G.A., et al. (1997). Oncostatin M is a proinflammatory mediator. In vivo effects correlate with endothelial cell expression of inflammatory cytokines and adhesion molecules. *The Journal of Clinical Investigation* 100(1)**,** 158-168. doi: 10.1172/JCI119508.

Navaratna, D., Guo, S., Arai, K., and Lo, E.H. (2009). Mechanisms and targets for angiogenic therapy after stroke. *Cell adhesion & migration* 3(2)**,** 216-223. doi: 10.4161/cam.3.2.8396.

Ng, D.C.H., Lin, B.H., Lim, C.P., Huang, G., Zhang, T., Poli, V., et al. (2006). Stat3 regulates microtubules by antagonizing the depolymerization activity of stathmin. *The Journal of cell biology* 172(2)**,** 245-257. doi: 10.1083/jcb.200503021.

Potente, M., and Carmeliet, P. (2017). The Link Between Angiogenesis and Endothelial Metabolism. *Annu Rev Physiol* 79**,** 43-66. doi: 10.1146/annurev-physiol-021115-105134.

Richards, C.D. (2013). The enigmatic cytokine oncostatin m and roles in disease. *ISRN Inflamm* 2013**,** 512103. doi: 10.1155/2013/512103.

Sergushichev, A.A. (2016). An algorithm for fast preranked gene set enrichment analysis using cumulative statistic calculation. *bioRxiv***,** 060012. doi: 10.1101/060012.

Sun, D., Li, S., Wu, H., Zhang, M., Zhang, X., Wei, L., et al. (2015). Oncostatin M (OSM) protects against cardiac ischaemia/reperfusion injury in diabetic mice by regulating apoptosis, mitochondrial biogenesis and insulin sensitivity. *Journal of cellular and molecular medicine* 19. doi: 10.1111/jcmm.12501.

Teng, T.S., Lin, B., Manser, E., Ng, D.C.H., and Cao, X. (2009). Stat3 promotes directional cell migration by regulating Rac1 activity via its activator βPIX. *Journal of cell science* 122(22)**,** 4150-4159.

Timofeeva, O.A., Chasovskikh, S., Lonskaya, I., Tarasova, N.I., Khavrutskii, L., Tarasov, S.G., et al. (2012). Mechanisms of unphosphorylated STAT3 transcription factor binding to DNA. *J Biol Chem* 287(17)**,** 14192-14200. doi: 10.1074/jbc.M111.323899.

Vasse, M., Pourtau, J., Trochon, V., Muraine, M., Vannier, J.-P., Lu, H., et al. (1999). Oncostatin M induces angiogenesis in vitro and in vivo. *Arteriosclerosis, thrombosis, and vascular biology* 19(8)**,** 1835-1842.

Viallard, C., and Larrivée, B. (2017). Tumor angiogenesis and vascular normalization: alternative therapeutic targets. *Angiogenesis* 20(4)**,** 409-426. doi: 10.1007/s10456-017-9562-9.

Wegrzyn, J., Potla, R., Chwae, Y.-J., Sepuri, N.B., Zhang, Q., Koeck, T., et al. (2009). Function of mitochondrial Stat3 in cellular respiration. *Science* 323(5915)**,** 793-797.

Wolf, D., and Ley, K. (2019). Immunity and Inflammation in Atherosclerosis. *Circ Res* 124(2)**,** 315-327. doi: 10.1161/circresaha.118.313591.

Yu, G., and He, Q.-Y. (2016). ReactomePA: an R/Bioconductor package for reactome pathway analysis and visualization. *Molecular BioSystems* 12(2), 477-479.

Yu, G., Wang, L.-G., Han, Y., and He, Q.-Y. (2012). clusterProfiler: an R Package for Comparing Biological Themes Among Gene Clusters. *OMICS: A Journal of Integrative Biology* 16(5), 284-287. doi: 10.1089/omi.2011.0118.

Zhang, N., Ma, D., Wang, L., Zhu, X., Pan, Q., Zhao, Y., et al. (2017). Insufficient Radiofrequency Ablation Treated Hepatocellular Carcinoma Cells Promote Metastasis by Up-Regulation ITGB3. *Journal of Cancer* 8(18), 3742-3754. doi: 10.7150/jca.20816.

Zhang, Q., Raje, V., Yakovlev, V.A., Yacoub, A., Szczepanek, K., Meier, J., et al. (2013). Mitochondrial localized Stat3 promotes breast cancer growth via phosphorylation of serine 727. *Journal of Biological Chemistry* 288(43), 31280-31288.

Zhang, X., Zhu, D., Wei, L., Zhao, Z., Qi, X., Li, Z., et al. (2015). OSM Enhances Angiogenesis and Improves Cardiac Function after Myocardial Infarction. *BioMed Research International* 2015, 317905. doi: 10.1155/2015/317905.

Zhu, M., Che, Q., Liao, Y., Wang, H., Wang, J., Chen, Z., et al. (2015). Oncostatin M activates STAT3 to promote endometrial cancer invasion and angiogenesis. *Oncol Rep* 34(1), 129-138. doi: 10.3892/or.2015.3951.

Figures

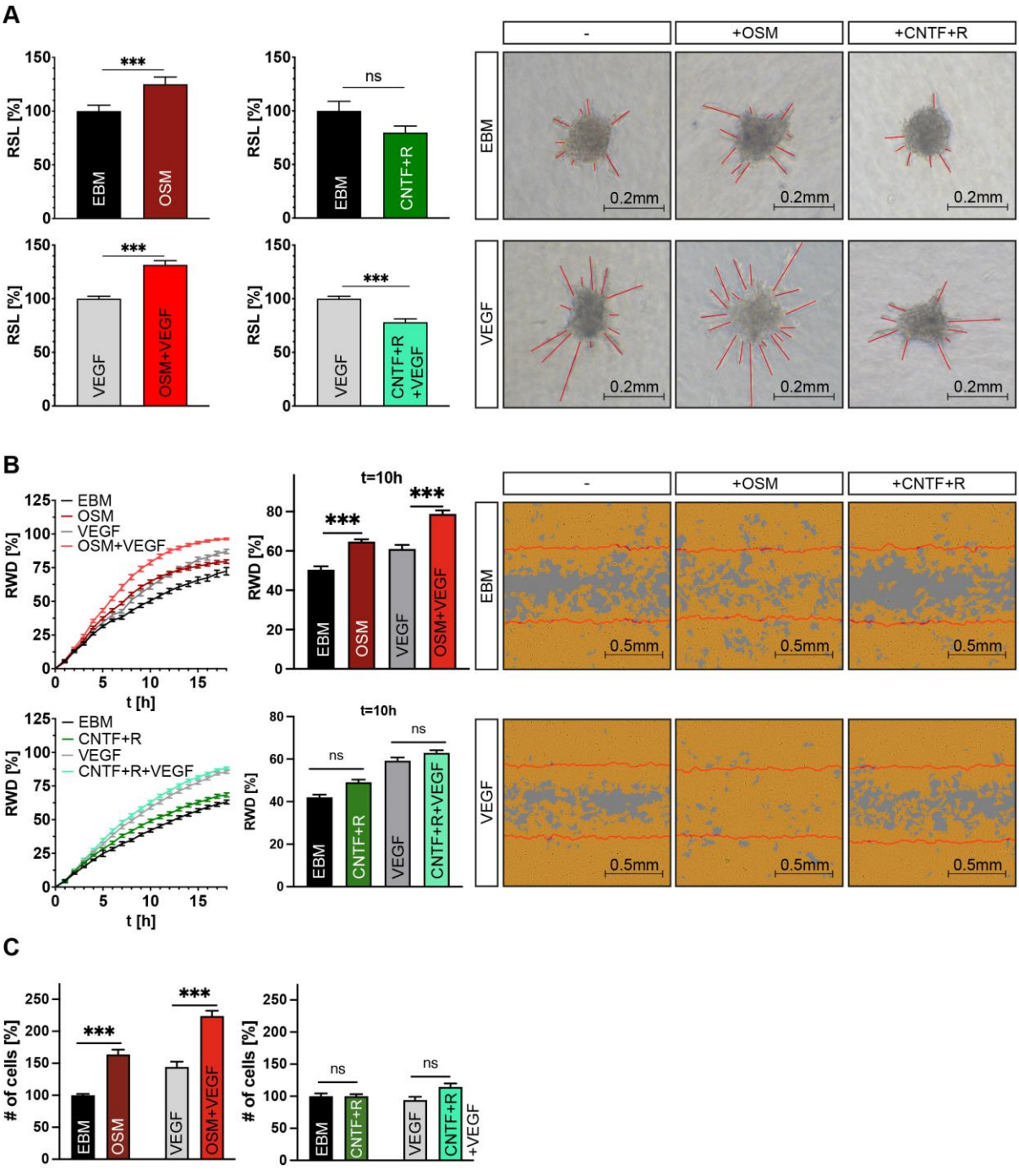

Fig. 1. OSM shows pro-angiogenic potential by activation of a broader range of signaling pathways in contrast to the anti-angiogenic CNTF+R. (**A**) Relative sprouting length (RSL) of HUVECs stimulated by Endothelial Basal Medium (EBM) as negative control, OSM, and CNTF+R with or without VEGF measured in the spheroid sprouting assay. N = 3-5 independent experiments with 12-20 spheroids

per group and experiment. A Mann–Whitney U Test was used for statical analysis. (**B**) Relative wound density (RWD) was measured over 18h to determine the migratory effect of EBM, OSM, CNTF+R or VEGF on HUVECs in the scratch wound assay. N = 3 independent experiments each including 6-8 technical replicates. A Kruskal–Wallis Test, adjusted for multiple testing determined significance 10 h after the start of the experiment. (C) Proliferation assay of HUVECs stimulated by specific cytokine treatment for 3 days. N = 3 independent experiments, Data is representative for three independent experiments with eight technical replicates each. A Kruskal–Wallis Test, adjusted for multiple testing determined significance.

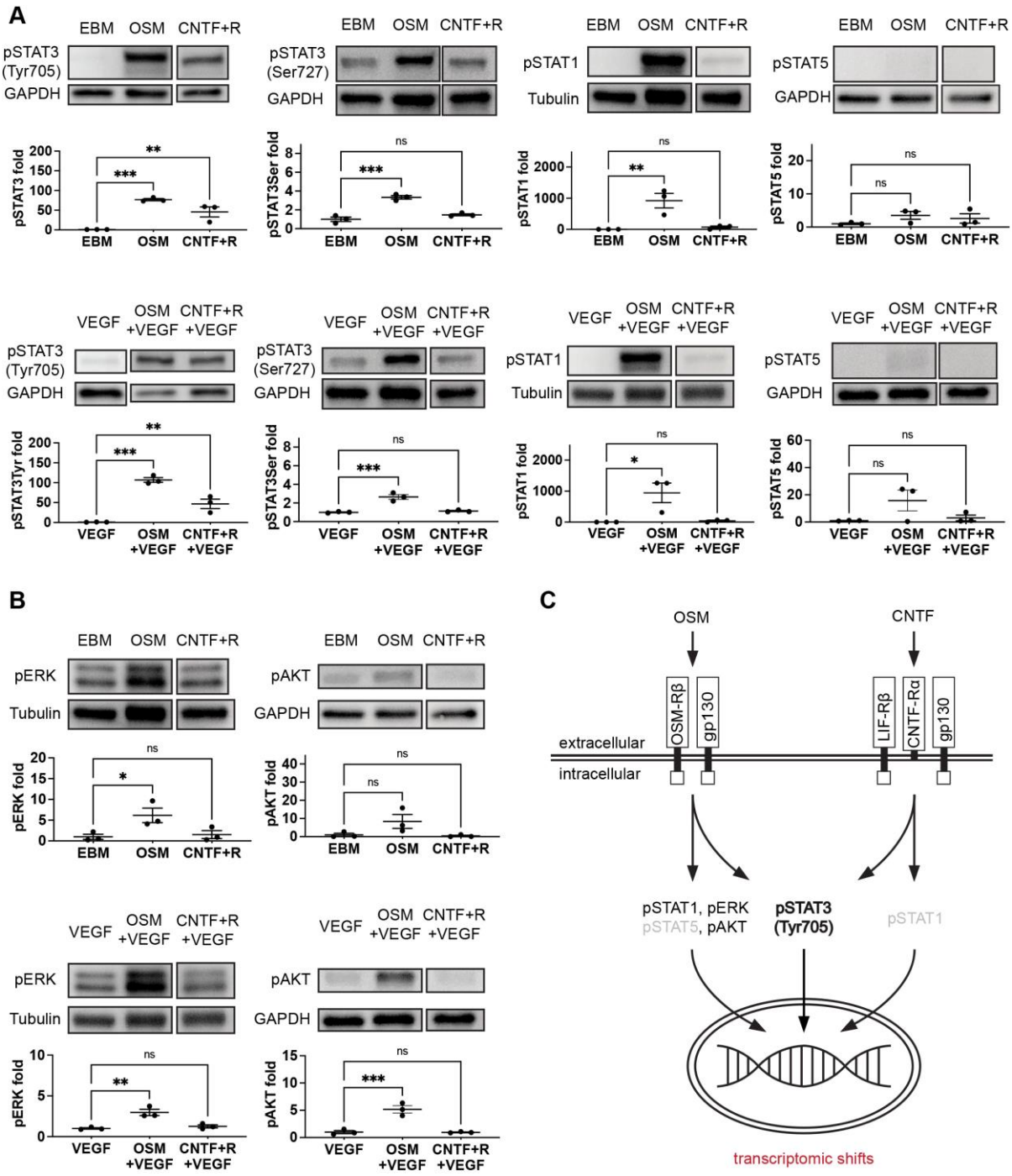

Fig. 2. OSM activates multiple other pathways beyond STAT3 in contrast to CNTF+R. (**A**) Western blot analysis of HUVECs stimulated by EBM or cytokines for activation of STAT related pathways. Protein lysates were collected after 15 min of stimulation except for the pSTAT3 Ser272 blot for which cells were incubated for 30 min. Statistical significance was calculated by an one-way ANOVA adjusted for multiple testing. (**B**) Western blot analysis of HUVECs stimulated by EBM or cytokines for activation of the ERK und AKT pathways. Protein lysates were

collected after 15 min of stimulation. Statistical significance was calculated by an ordinary one-way ANOVA adjusted for multiple testing. (**D**) Graphical summary of the activated pathways by OSM or CNTF+R as measured in the signaling analysis.

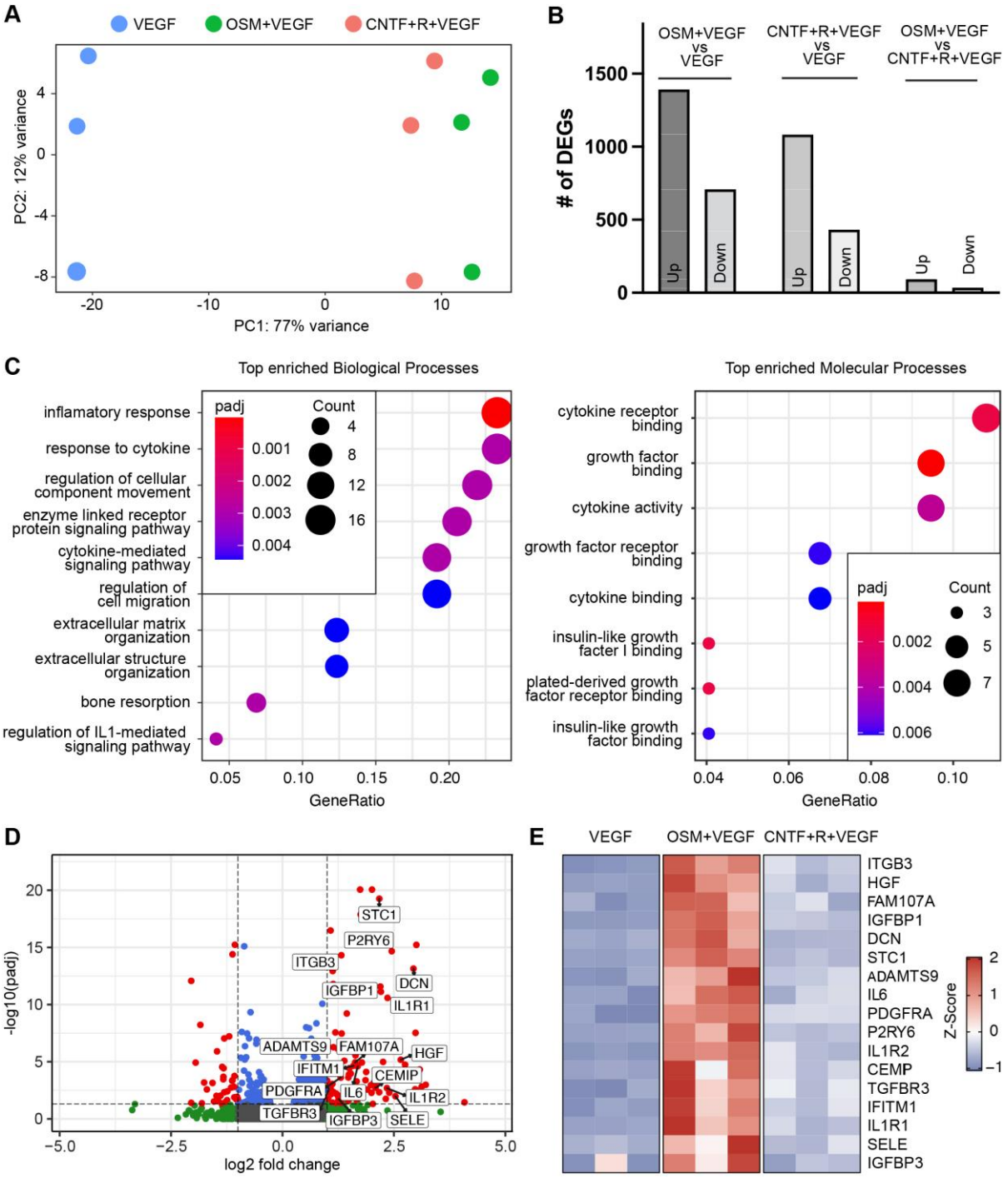

Fig. 3. The diverse angio-modulatory effect of OSM and CNTF+R on HUVECs corresponds to a distinct transcriptomic shift. (**A**) PCA of the HUVEC transcriptome following treatment with VEGF, VEGF+OSM and CNTF+R+VEGF for 24h. (**B**) Bar graph visualizing the amount of DEGs measured for each condition. (**C**) Gene ontology (GO) enrichment analysis of DEGs enriched for HUVECs treated with OSM+VEGF in contrast to CNTF+R+VEGF. The ten most significant GO terms according to the adjusted p value are shown and ranked based on their share at the

total number of DEGs (GeneRatio). Diagrams show terms enriched for OSM+VEGF and therefore depleted for CNTF+R+VEGF. The number of DEGs and the total number of genes for each GO-term can be found in Supplementary Table S3-4 (**D**) Volcano plot of all genes with at least one count in both samples of HUVECs treated with OSM+VEGF or CNTF+R+VEGF. Genes defined as upregulated DEGs after OSM+VEGF treatment are marked in red. Genes which were not considered differentially expressed due to a log2 fold change of < abs(1) although padj < 0.05 are colored blue. Features with a log 2-fold change > 1 but padj > 0.05 are marked green. Genes annotated with GO terms “regulation of cell migration” (GO: 0030334), “growth factor binding” (GO:0019838) or “growth factor receptor binding” (GO:0070851) are labelled. (**E**) Heatmap of the Z-Score of all labelled genes in (D) visualizing the three replicates of each condition.

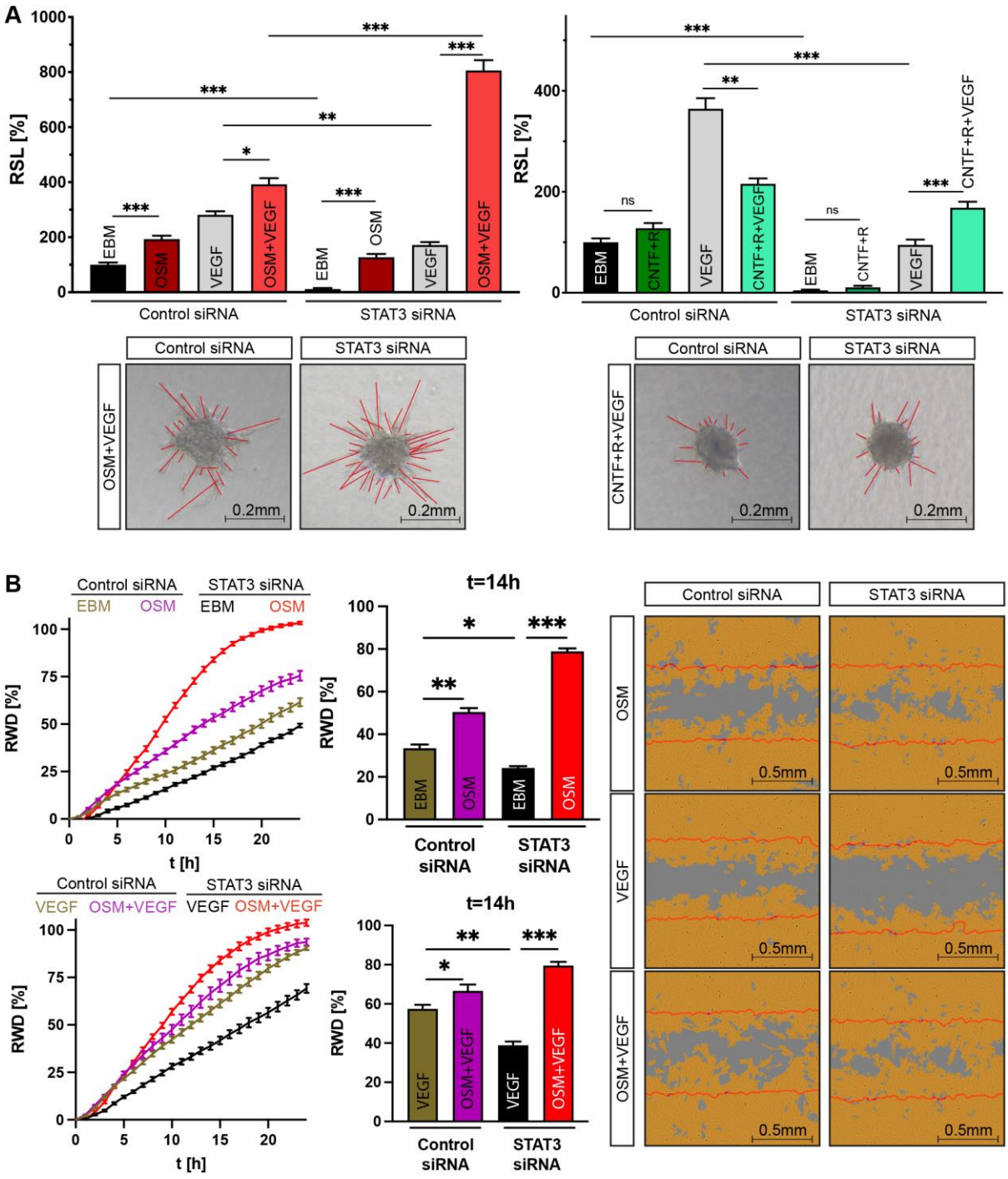

Fig. 4. STAT3 knock-down enhances OSM's pro-angiogenic effect and abolishes CNTF's anti-angiogenic influence on HUVECs. (**A**) Endothelial sprouting of HUVECs in response to EBM control, OSM, CNTF+R, VEGF, or a combination of the above was measured by the Relative Sprouting Length (RSL) in the spheroid sprouting assay following STAT3 knock-down and compared to controls treated with control siRNA. Data are representative of 3 independent experiments each consisting of 12-20 spheroids per group and experiment. Statistical testing was

conducted by a Kruskal–Wallis Test adjusted for multiple testing. (**B**) Relative Wound Density (RWD) of HUVECs in response to stimulation with EBM, OSM, VEGF or a combination was determined in the scratch wound assay of HUVECs transfected with STAT3 siRNA or control siRNA. N = 3 individual experiments which include 6-8 technical replicates each. A Kruskal–Wallis Test adjusted for multiple testing determined significance 14 h after stimulation.

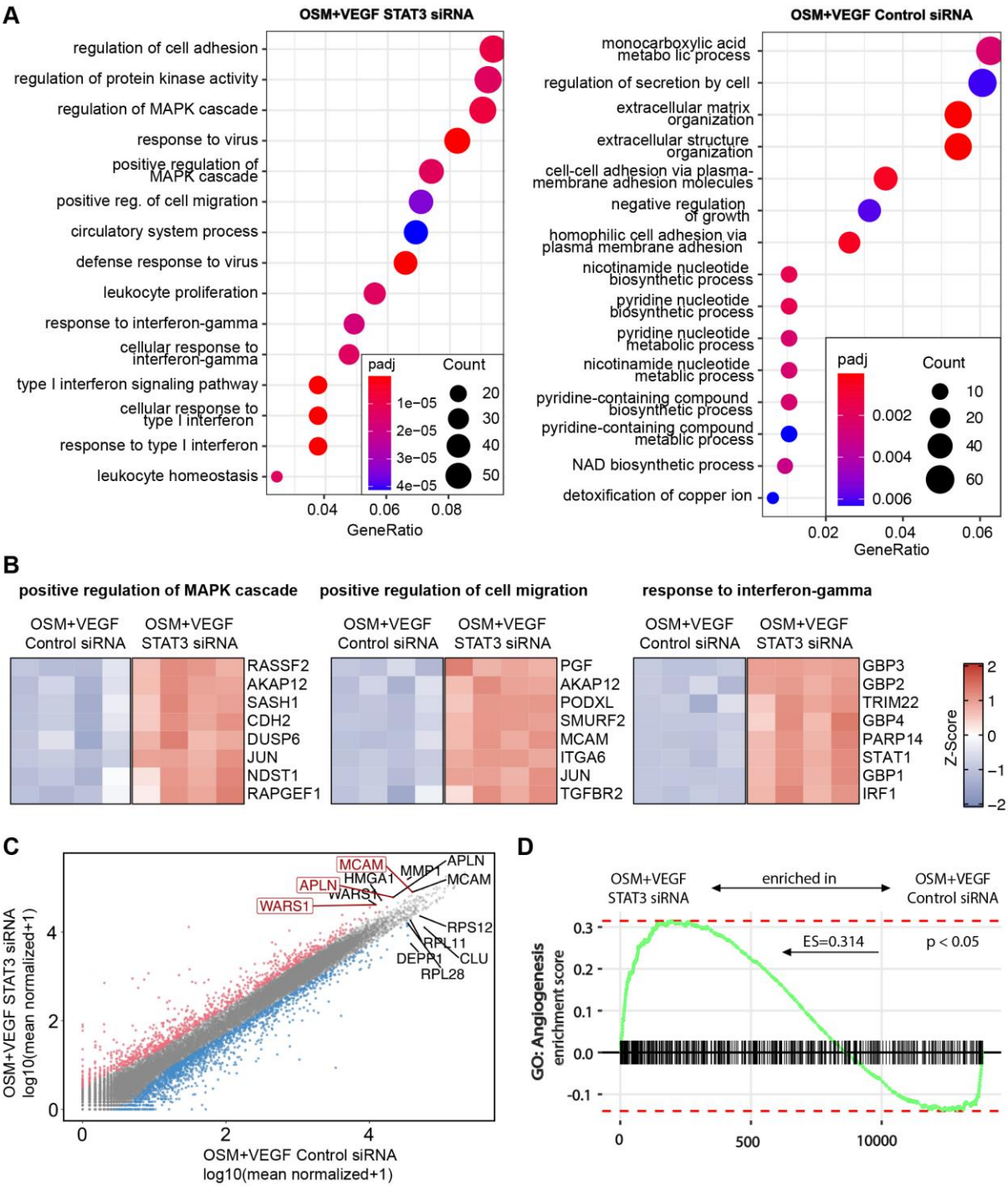

Fig. 5. STAT3 knock-down in HUVECs induces a transcriptomic shift towards a dysregulated state of proliferation, migration and vascular development in response to OSM treatment including an upregulation of ERK and STAT1-associated signaling pathways on RNA level. (**A**) GO term enrichment analysis of DEGs enriched for HUVECs treated with OSM+VEGF following STAT3 knock-down (STAT3 siRNA) or treatment with control siRNA. The 15 statistically most significant GO terms according to the adjusted p value are shown and ranked by their share of

the total number of DEGs (GeneRatio). The diagrams show the enriched terms for the labeled condition. The number of DEGs and the total number of genes for one of the GO-terms can be found in in Supplementary Table S5-6 (**B**) Heatmaps of the 8 most expressed DEG tagged to GO terms associated with positive regulation of MAPK signaling (GO:0043410), response to IFNG pathway (GO:0034341) and positive regulation of cell migration (GO:0030335) visualized by the Z-Score in each replicate. (**C**) Scatterplot of all genes with at least one count in HUVECs treated with OSM +VEGF following STAT3 knock-down compared to the control siRNA group. Genes defined as upregulated DEGs in response to OSM +VEGF treatment following STAT3 knock-down are marked in red, differentially downregulated genes are marked in blue. The top 5 up- and downregulated DEGs according to their absolute expression are labeled. Genes which are related to GO term angiogenesis (GO:0001525) are highlighted. (**B**) GSEA for GO angiogenesis (GO:0001525) in HUVECs treated with OSM+VEGF following STAT3 knock-down.

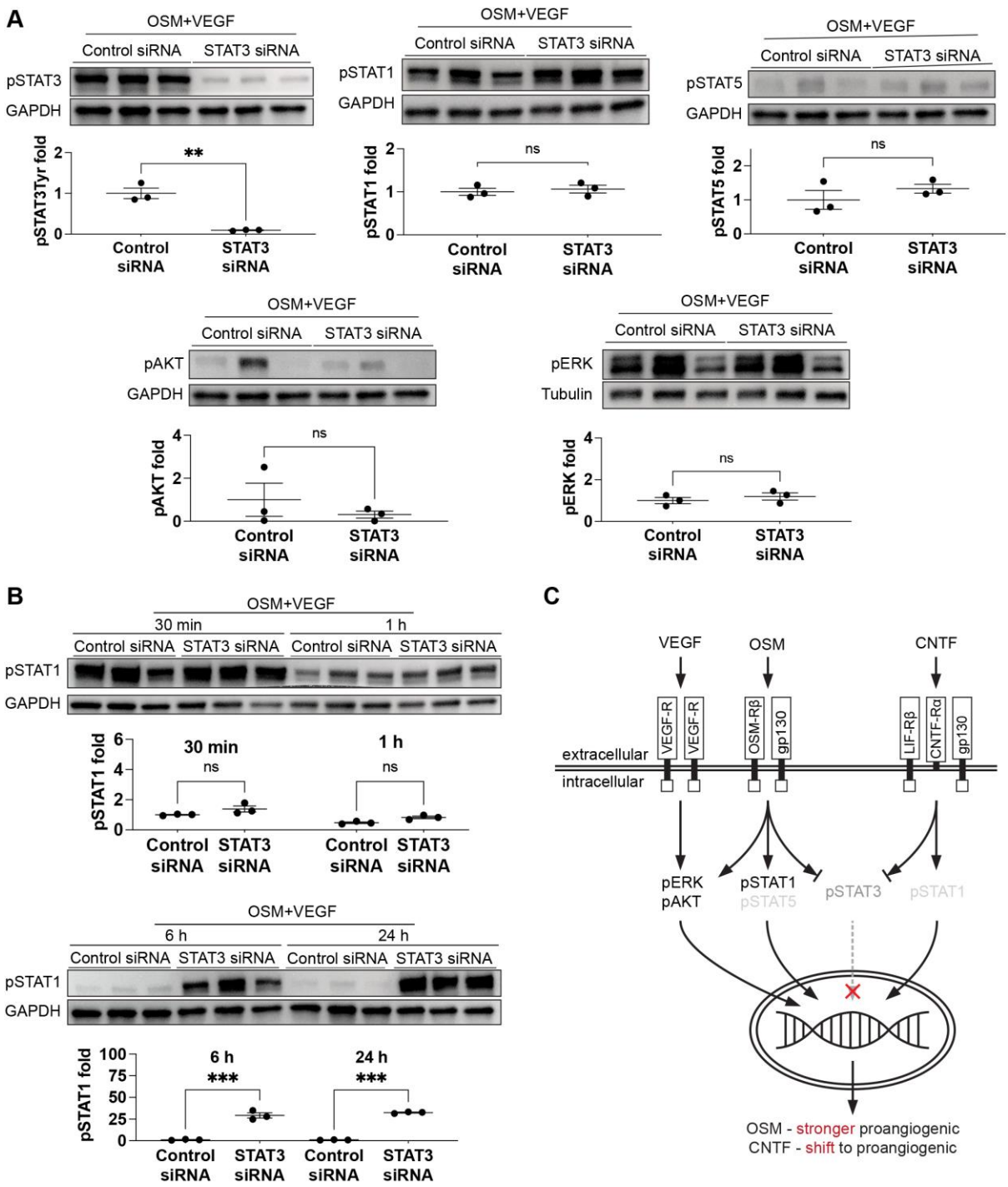

Fig. 6. Compensatory changes of intracellular signaling pathways in response to STAT3 knock-down and OSM+VEGF treatment. (**A**) Comparison of intracellular signaling patterns in HUVECs after successful STAT3 knock-down and treatment with different cytokines for 5 min using western blot. N = 3 independent experiments, statistical testing: unpaired student t test. (**B**) Western blot analysis for pSTAT1 at 30 min, 1 h, 6 h and 24 h in OSM+VEGF treated HUVECs with or without STAT3 knock-

down. N = 3 independent experiments. statistical testing: unpaired student t test. (**C**) Graphical summary of the altered signaling patterns by OSM and CNTF+R and how the angiogenic phenotype changed due to knock-down.

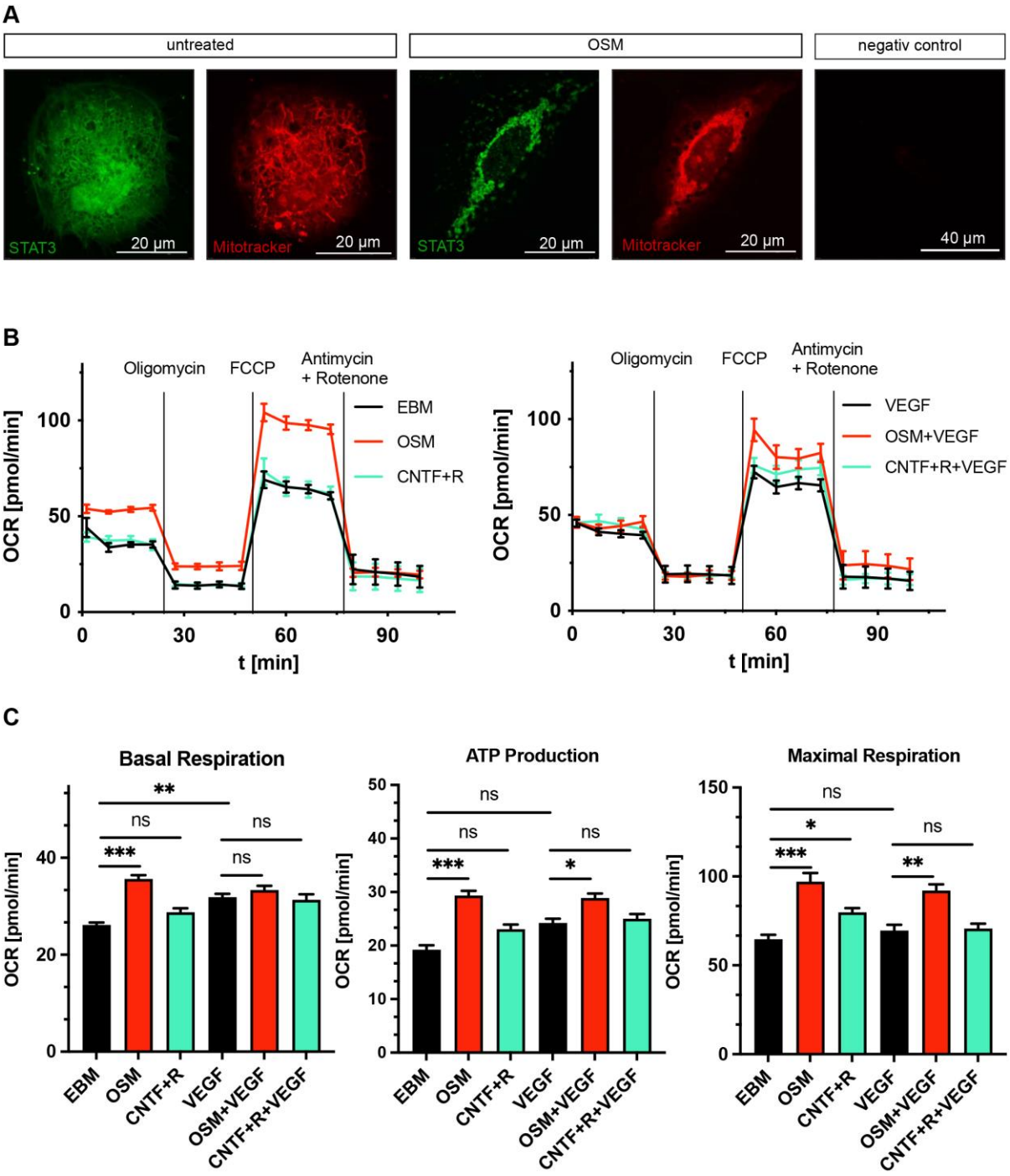

Fig. 7. STAT3 accumulates in mitochondria after OSM treatment and increases mitochondrial activity.

(**A**) Immunocytochemical analysis of BAECs transfected with Venus-WTSTAT3 plasmids. BAECs were stimulation with OSM or negative control for 30 min and stained with Mitotracker. Negative control refers to BAECs transfected with no plasmid and no incubation with Mitotracker. (**B**) Representative graphs of the oxygen consumption rate (OCR) of HUVECs pretreated overnight with different cytokines or

EBM using Seahorse XF Cell Mito Stress Test. Each graph includes 6-8 technical replicates. Data is normalized to the measured cell count in each well. (**C**) Normalized quantification of the Seahorse XF Cell Mito Stress Test results from HUVECs pretreated with cytokines or EBM overnight. Data are representative of 3 independent experiments including 6-8 technical replicates each. A Kruskal Wallis adjusted for multiple testing was used for statistical analysis.

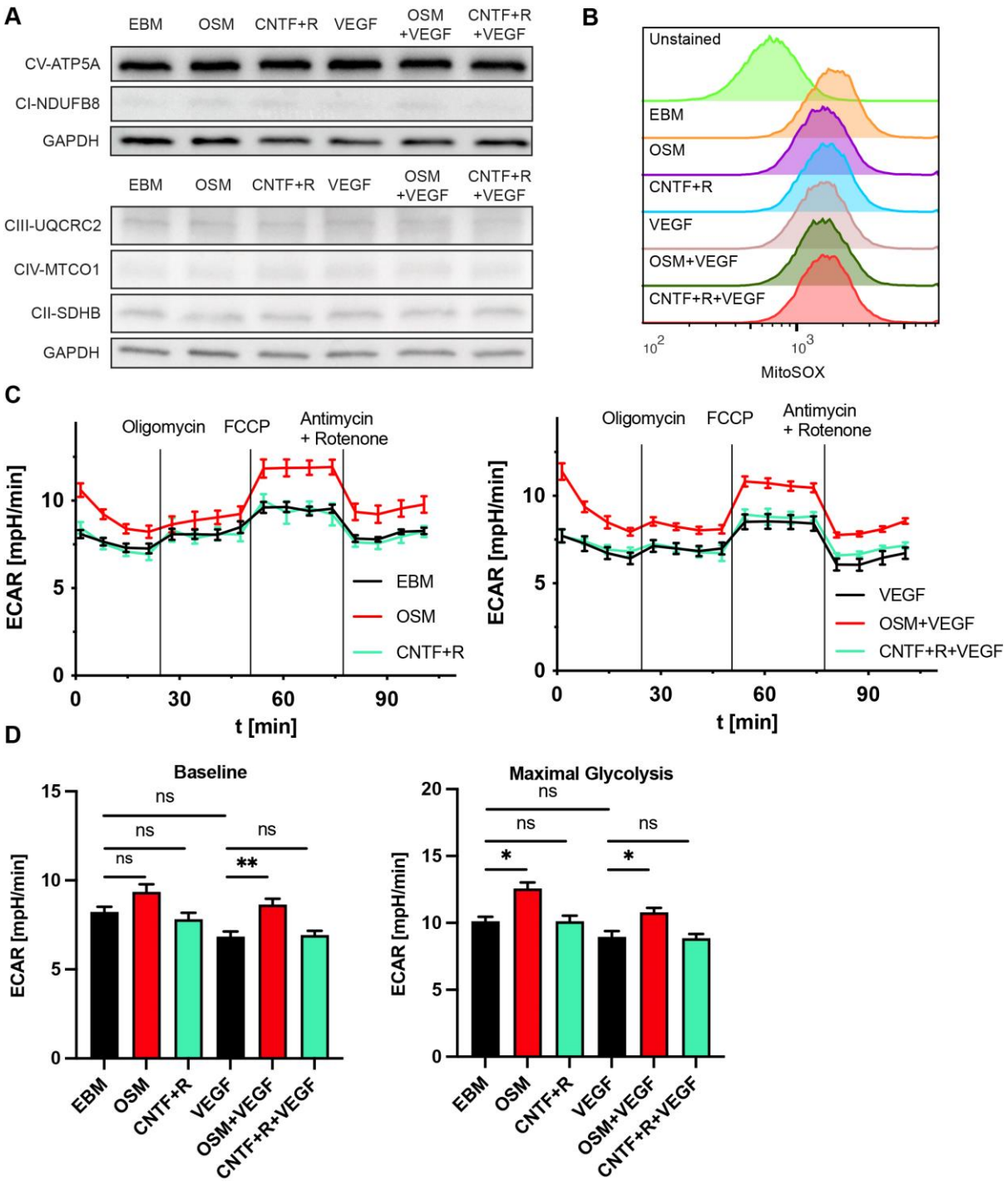

Fig. 8. Analysis of metabolic changes induced by OSM or CNTF+R treatment in HUVECs.

(**A**) Western blot analysis of the expression of mitochondrial complex I (CI-NDUFB8), complex II (CII-SDHB), complex III (CIII-UQCRC2), complex IV (CIV-MTCO1) and complex V (CV-ATP5A) after overnight treatment with cytokines or EBM. (**B**) Exemplary flowcytometry measurements for the production of ROS after pretreatment of HUVECS with cytokines or EBM overnight using the MitoSOX assay.

(**C**) Representative graphs of the extracellular acidification rate (ECAR) of HUVECs pretreated overnight with EBM or different cytokines using Seahorse XF Cell Mito Stress Test. Each graph includes 6-8 technical replicates. Data is normalized to the measured cell count in each well. (**D**) Normalized quantification of the glycolytic activity of HUVECs pretreated with EBM or cytokines overnight. N = 3 independent experiments including 6-8 technical replicates each. A Kruskal Wallis test was used for statistical analysis and adjusted for multiple testing.

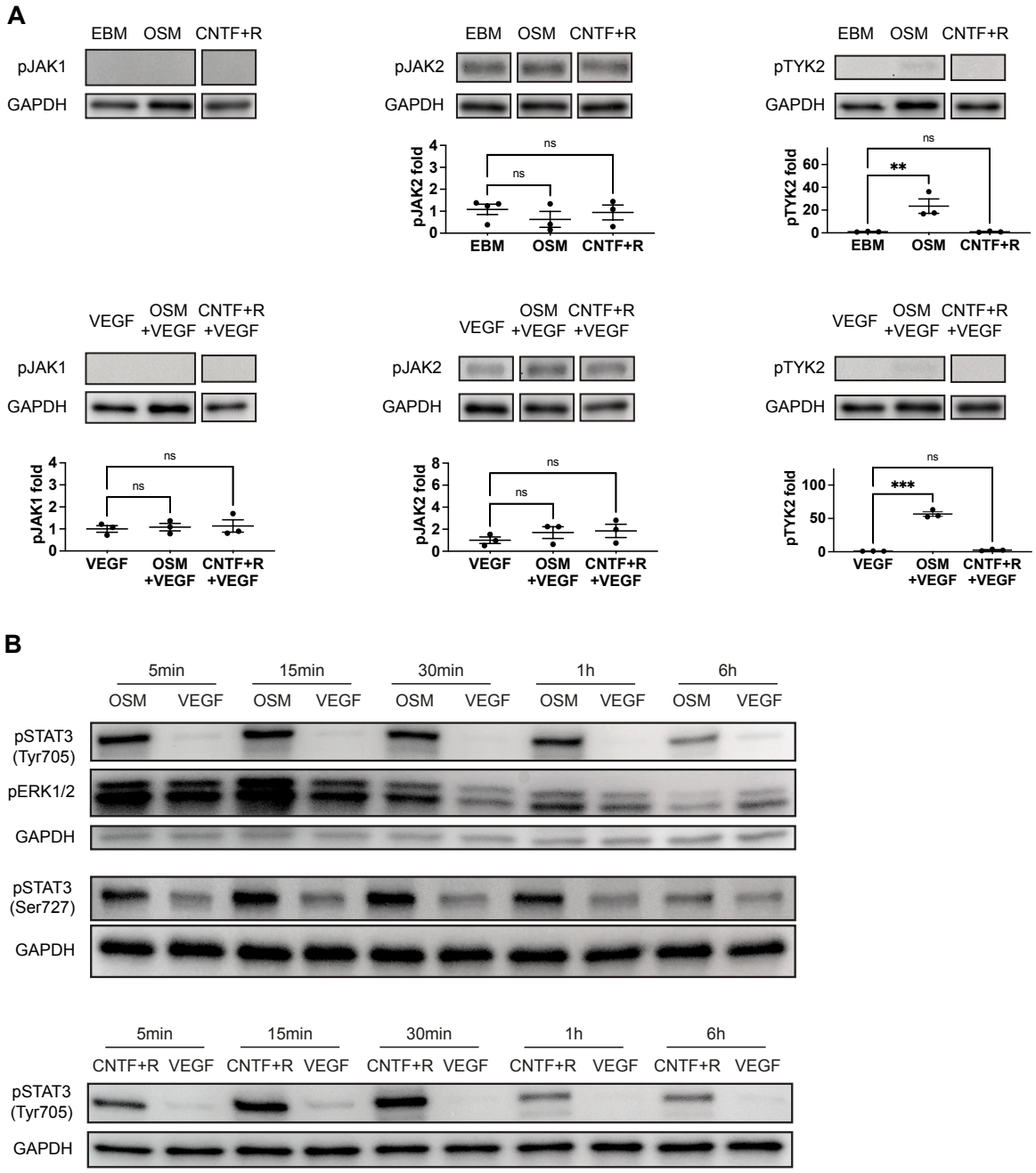

Fig. S1. JAK activation and time kinetic of pSTAT3 Tyr 705 activation in HUVECs following cytokine treatment. (**A**) Western blot analysis of HUVEC lysates stimulated by cytokines or EBM/VEGF as control for 5 min. Selected images show representative results. N = 3 biological replicates. * p< 0.05 one-way ANOVA adjusted for multiple testing. Uncut blots can be found in the supplementary material. (**B**) HUVECs were treated with VEGF, OSM or CNTF+R for up to 6 h and their potential to activate their respective pathways investigated by western blot.

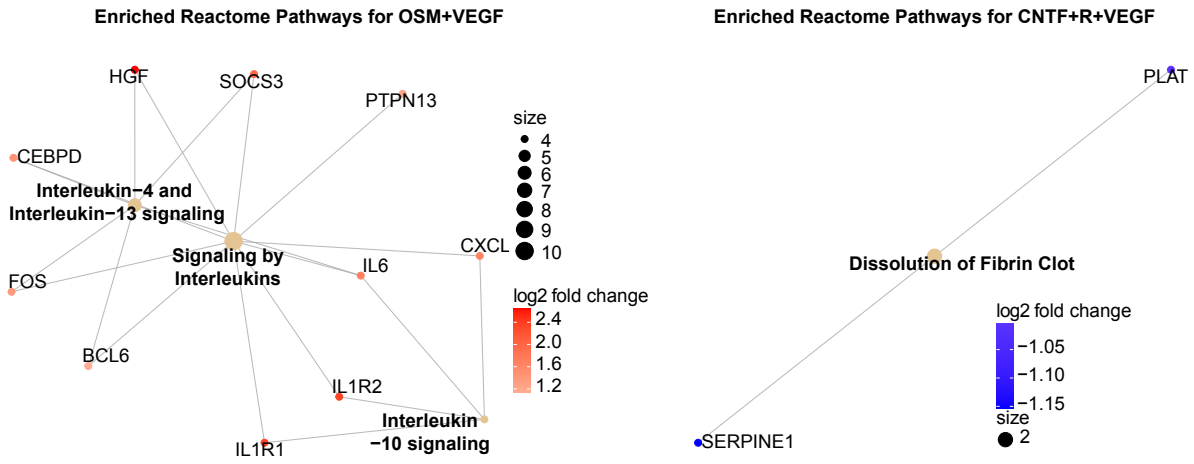

Fig. S2. Pathway enrichment analysis for DEGs of the RNA sequencing data of OSM+VEGF stimulated HUVECs in comparison to CNTF+R+VEGF treatment using the Reactome database. Size refers to the number of DEGs in the enriched pathway.

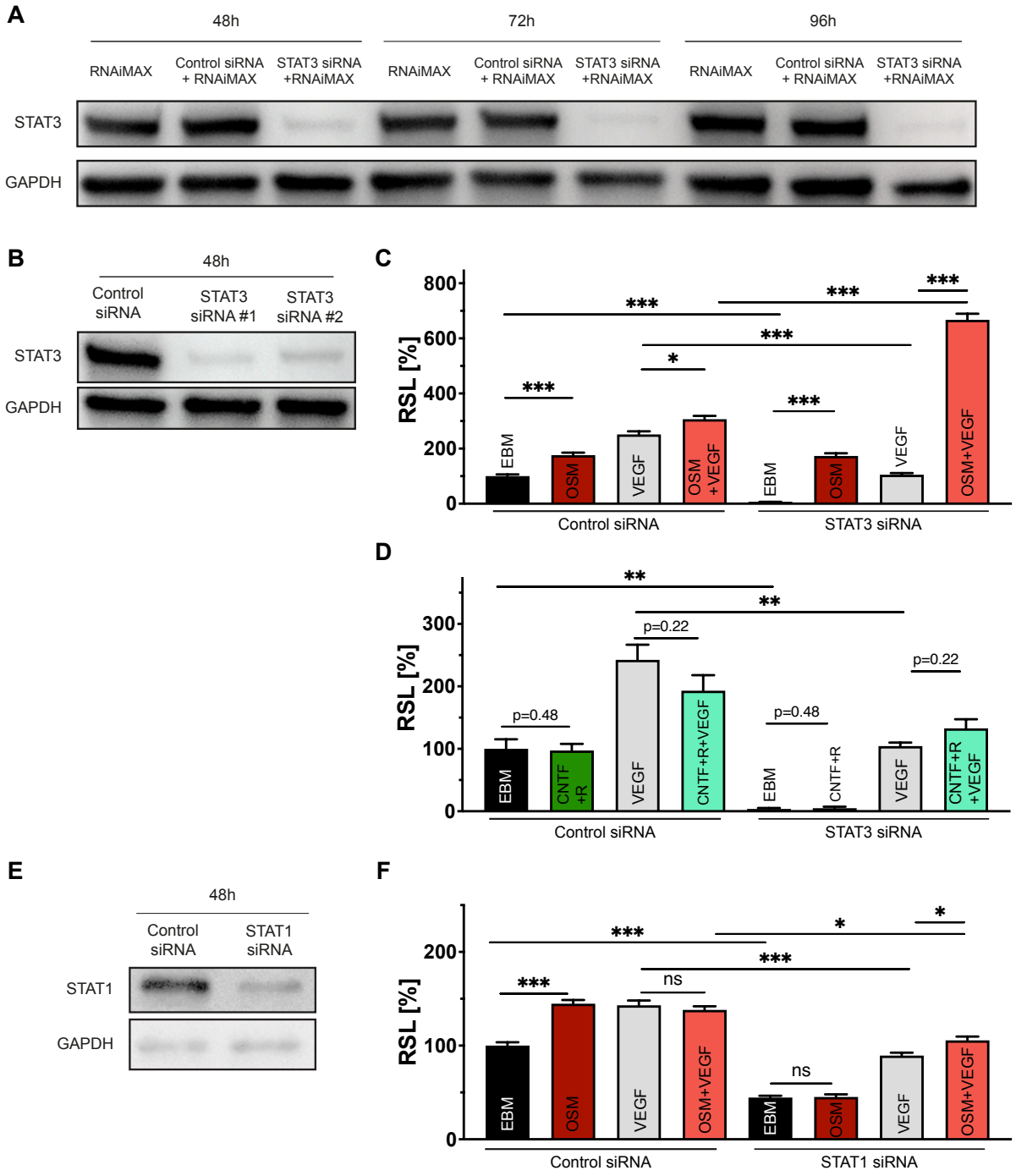

Fig. S3. Validation of STAT3 knock-down and on-target accuracy. (**A**) Western blot analysis of HUVECs transfected with plain RNAiMAX or in combination with Control siRNA or STAT3 siRNA. Time points refer to time passed after transfection. (**B**) Validation of a second STAT3 siRNA with a different target sequence using western blot. (**C**) Spheroid-Sprouting Assay of HUVECs transfected with the second STAT3 siRNA or Control siRNA treated with Endothelial Basel Medium (EBM), OSM, OSM+VEGF or VEGF. N = 3 independent experiments consisting of 12-20 spheroids

per group and experiment. Statistical testing: Kruskal–Wallis Test adjusted for multiple testing. (**D**) Spheroid-Sprouting Assay of HUVECs transfected with the second STAT3 siRNA or Control siRNA treated with Endothelial Basel Medium (EBM), CNTF+R, CNTF+VEGF or VEGF. N = 1 independent experiment consisting of 12-20 spheroids per group. A Kruskal–Wallis Test adjusted for multiple testing was used to determine statistical significance. (**D**) Western blot analysis to determine sufficient STAT1 knock-down in HUVECs 48 after transfection. (**E**) Spheroid-Sprouting Assay of HUVECs transfected with STAT1 siRNA or Control siRNA treated with Endothelial Basal Medium (EBM), OSM, OSM+VEGF or VEGF. N = 3 independent experiments consisting of 12-20 spheroids per group and experiment. Statistical testing: Kruskal–Wallis Test adjusted for multiple testing.

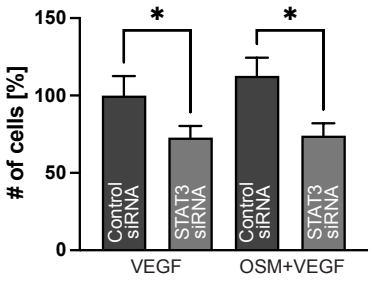

Fig. S4. Influence of STAT3 Knock-Down on OSM+VEGF induced proliferation. Proliferation assay of HUVECs with or without STAT3 knock-down stimulated with OSM+VEGF for 3 days. Data is representative for three independent experiments with 8 technical replicates each. A Kruskal-Wallis test adjusted for multiple testing was performed for statistical analysis.

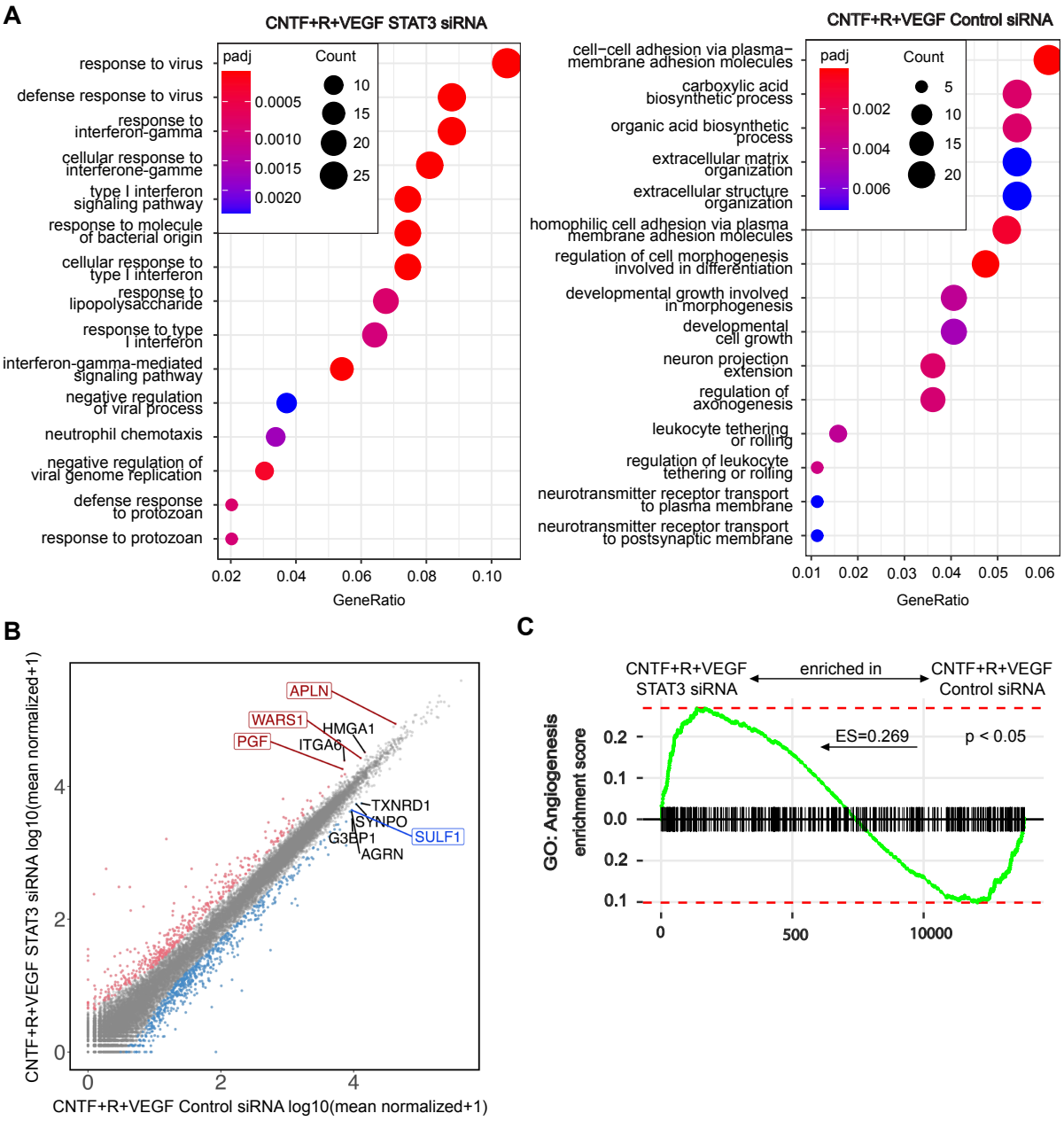

Fig. S5. The transcriptome of CNTF+R+VEGF stimulated STAT3 knock-down cells shows similarly tendencies as for OSM+VEGF stimulated STAT3 knock-down cells. (**A**) GO enrichment analysis for enriched biological processes between CNTF+R+VEGF stimulated HUVECs with or without STAT3 knock-down for each condition. The ten most significant enriched GO terms according to their adjusted p-value are shown and sorted based on their share at the total number of DEGs (GeneRatio). The diagrams show the enriched terms for the labeled condition. The number of DEGs and the total number of genes for one of the GO-terms can be found in Supplementary Table S7-8 (**B**) Scatterplot of all DEGs with at least one count in both groups comparing CNTF+R+VEGF stimulated HUVECs with or without

STAT3 knock-down. Genes defined as upregulated DEGs are labeled red and downregulated DEGs blue. The five most expressed DEGs from each category are highlighted by name and DEGs linked to the GO term Angiogenesis (GO:0001525) additionally highlighted. (**C**) GSEA between CNTF+R+VEGF HUVECs with or without STAT3 knock-down for the GO term Angiogenesis (GO:0001525). A positive enrichment score refers to enrichment for STAT3 knock-down cells stimulated with CNTF+R+VEGF.

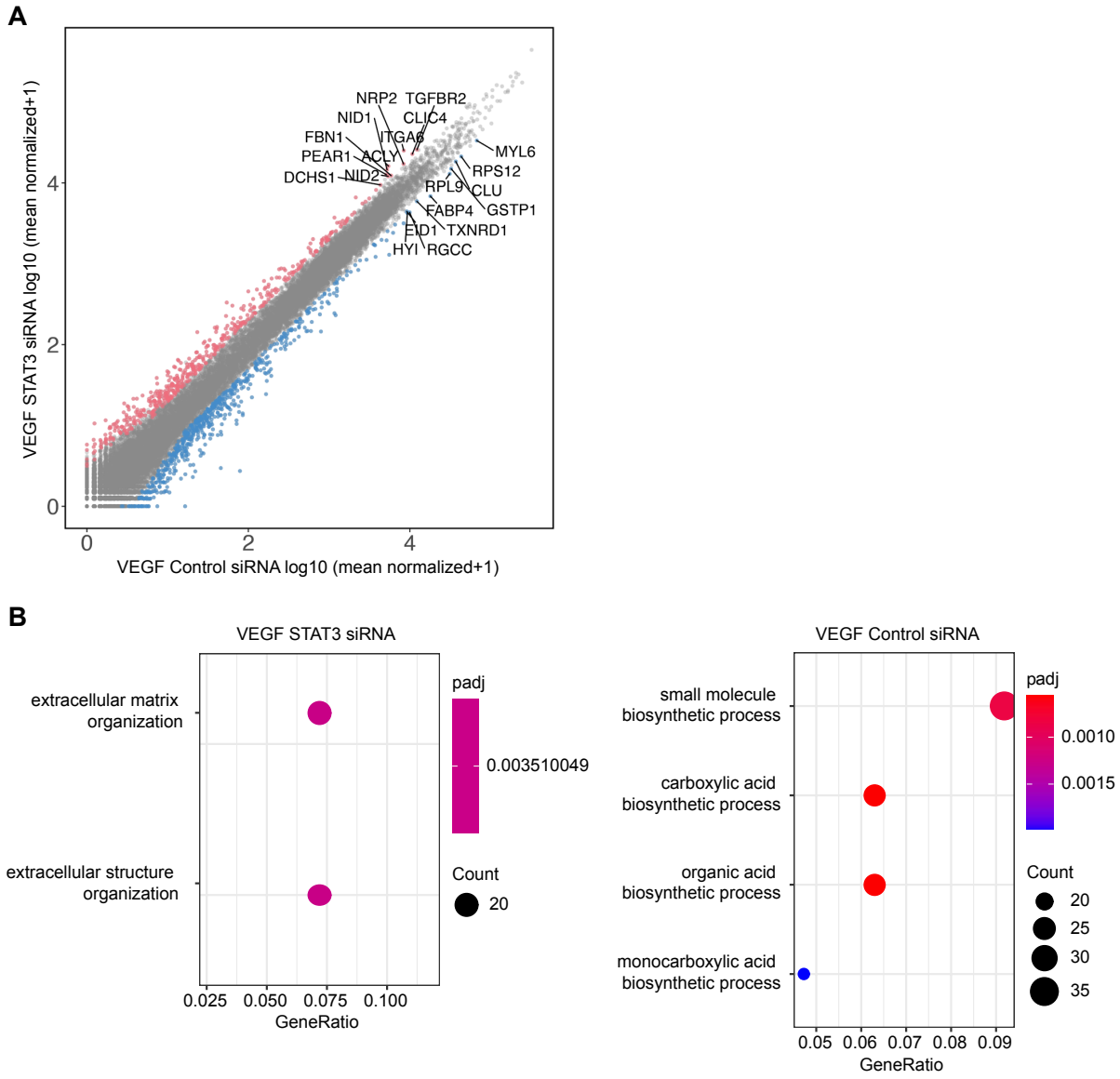

Fig. S6. STAT3 knock-down in VEGF stimulated HUVECs does not shift the transcriptome in a clear direction. (**A**) Scatterplot of all DEGs with at least one count in both groups comparing VEGF stimulated HUVECs with or without STAT3 knock-down. Genes defined as upregulated DEGs are labeled red and downregulated DEGs blue. The ten most expressed DEGs from each category are highlighted by name. (**B**) GO enrichment analysis for enriched biological processes between VEGF stimulated HUVECs with or without STAT3 knock-down for each condition. GO terms are ranked based on their share at the total number of DEGs (GeneRatio). The diagrams show the enriched terms for the labeled condition. The number of DEGs and the total number of genes for one of the GO-terms can be found in Supplementary Table S9-10.

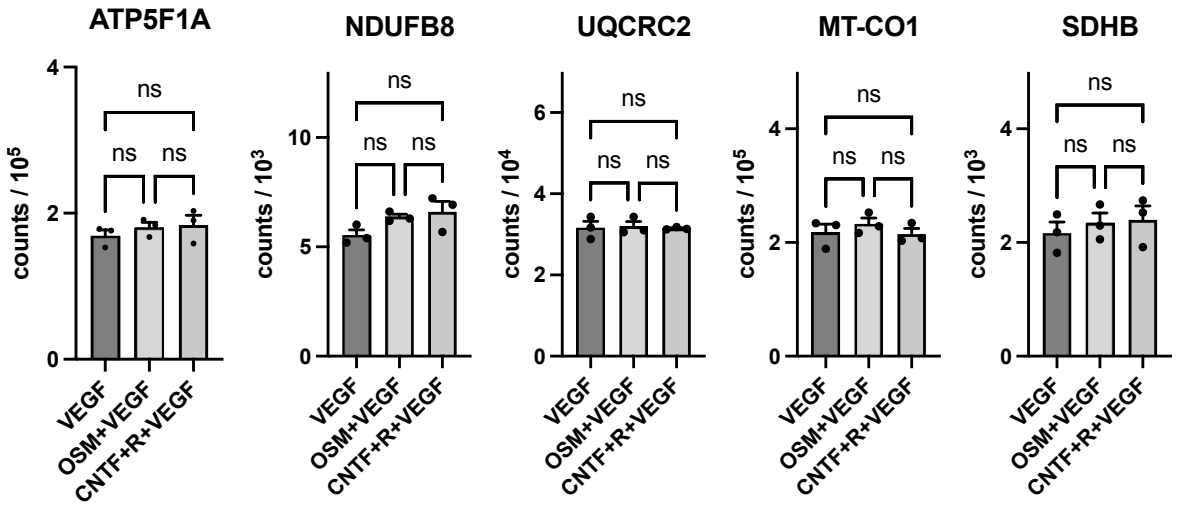

Fig. S7. RNA sequencing further validates the western blot analysis of mitochondrial complexes. Expression of different components of mitochondrial complexes in HUVECs stimulated with different cytokines for 24h according to RNASeq.

Fig. S8. Blot transparency

(**I**) pSTAT3Tyr, no co-stimulation with VEGF

(**II**) pSTAT3Ser, no co-stimulation with VEGF

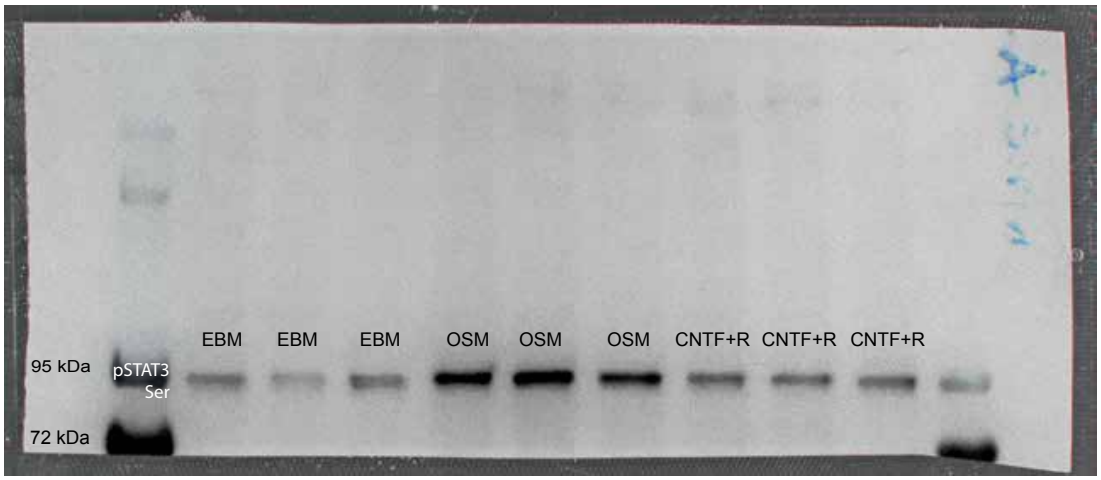

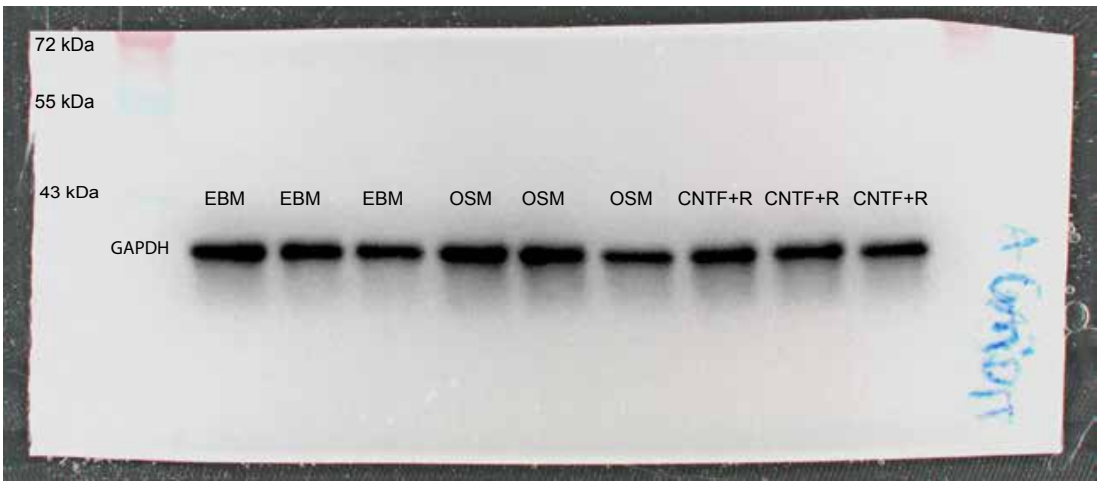

(**II**) pSTAT1, pERK, no co-stimulation with VEGF

(**III**) pSTAT5, pAKT, no co-stimulation with VEGF

(**IV**) pSTAT3Tyr, co-stimulation with VEGF

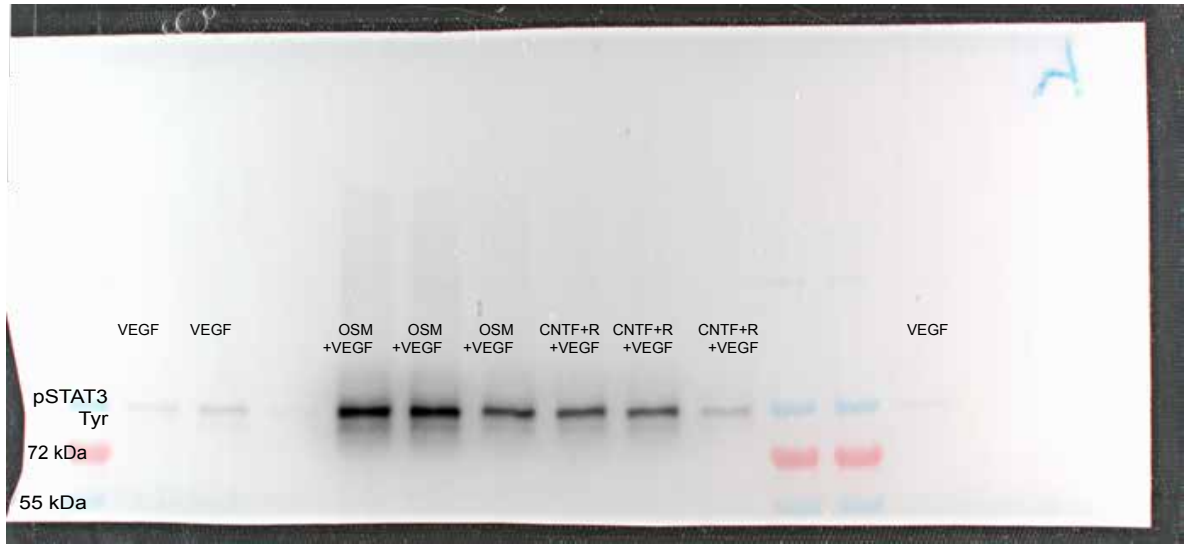

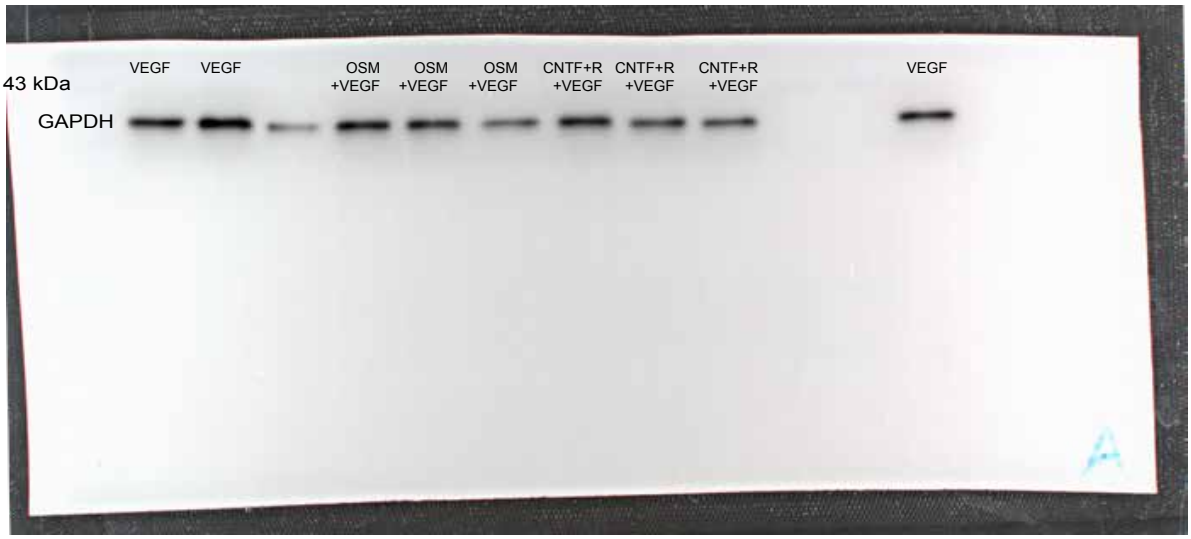

(**V**) pSTAT3Ser, co-stimulation with VEGF

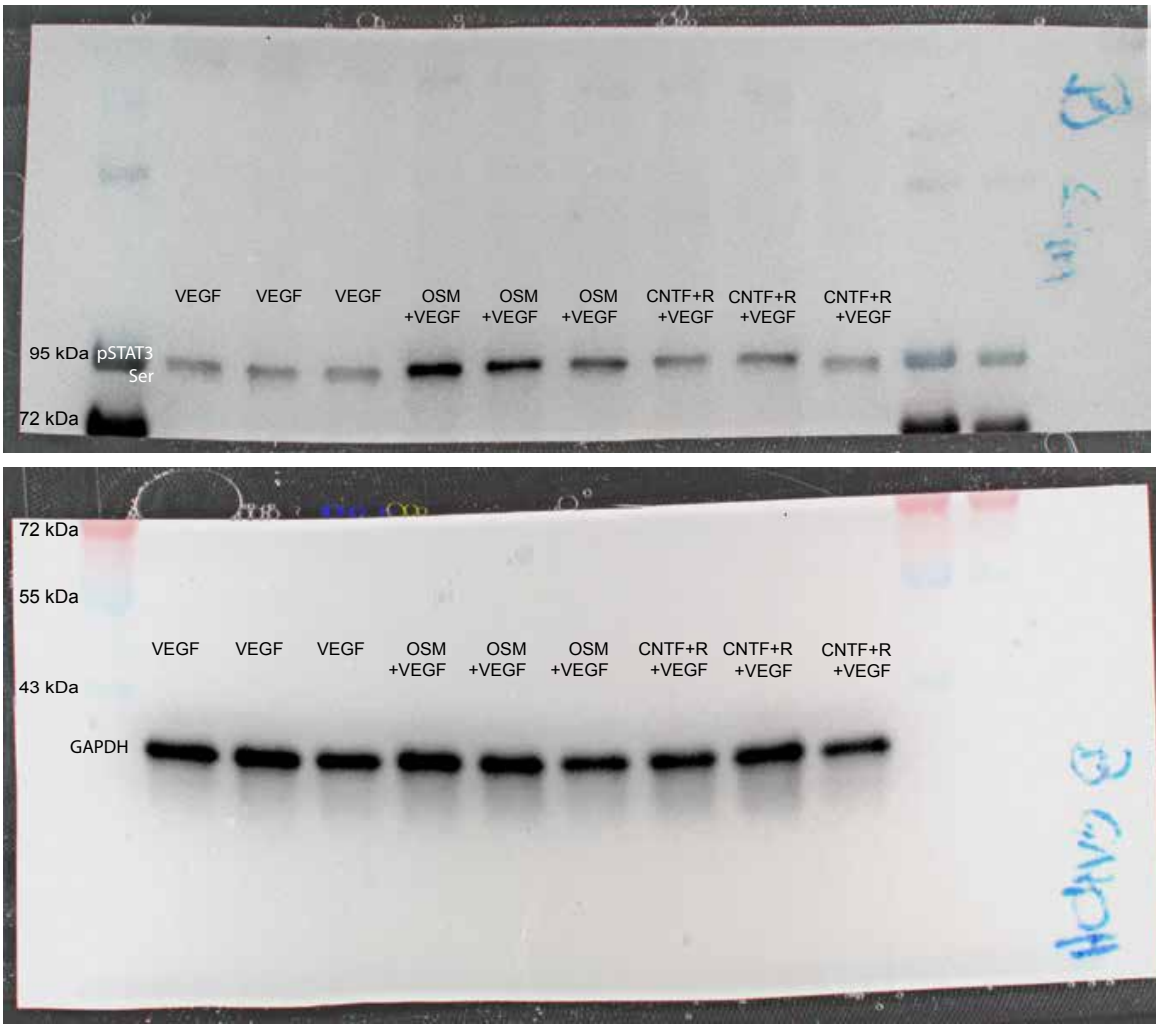

(**VI**) pSTAT1, co-stimulation with VEGF

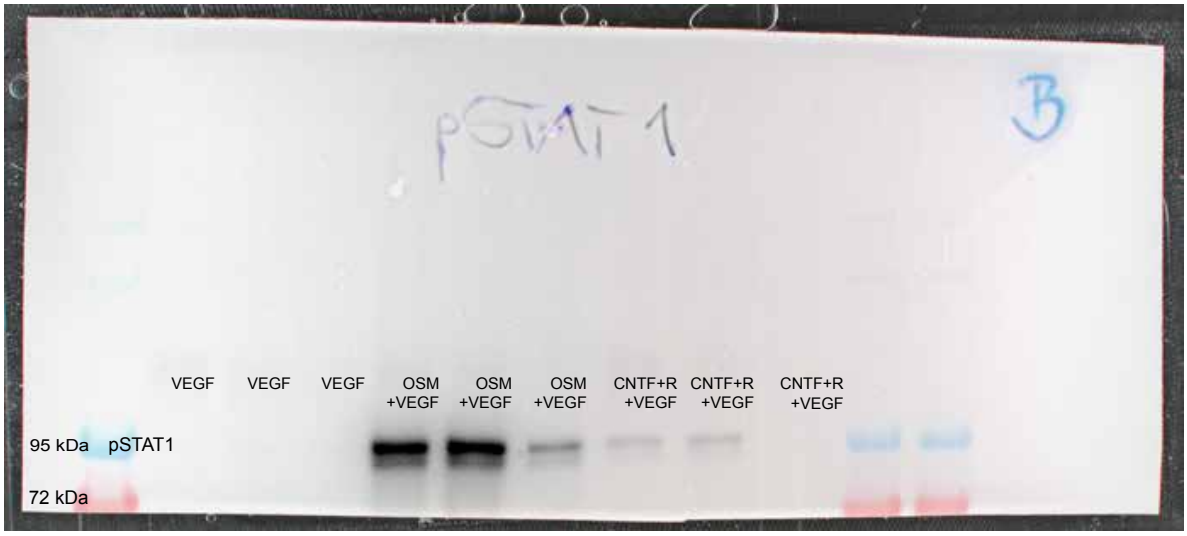

(**VII**) pSTAT5, pAKT, co-stimulation with VEGF

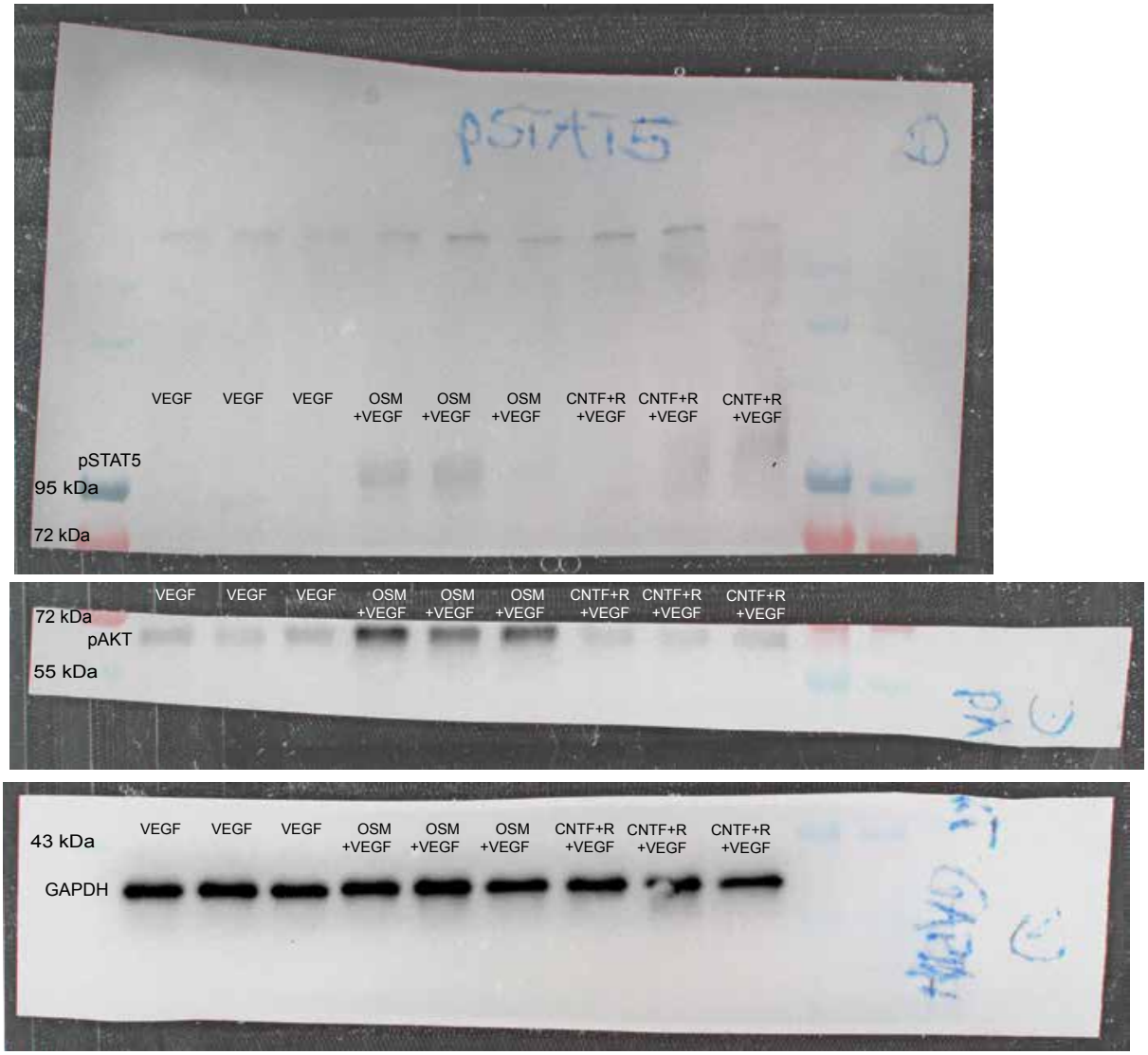

Fig. S9.

(**I**) STAT3 knock-down, OSM+VEGF (5 min), pSTAT3, pAKT

(**II**) STAT3 knock-down, OSM+VEGF (5 min), pSTAT1

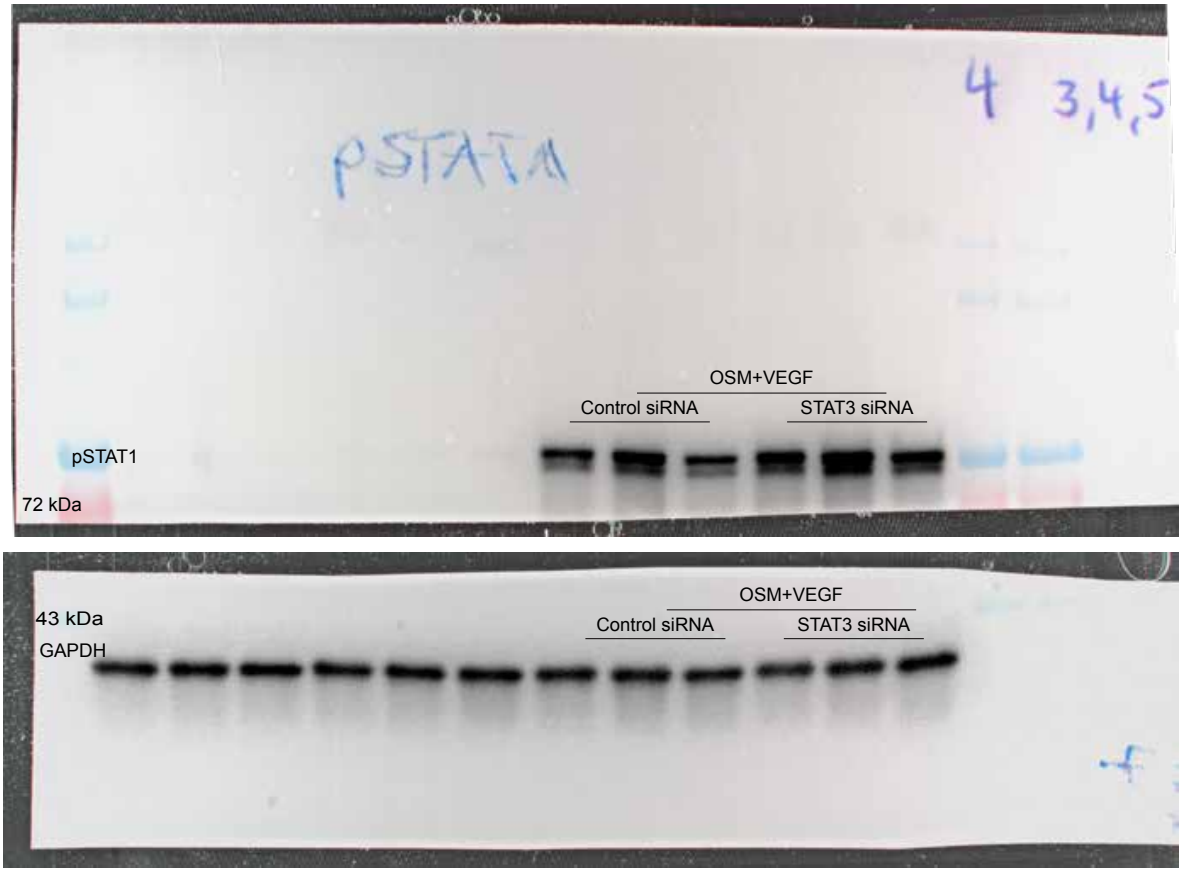

(**III**) STAT3 knock-down, OSM+VEGF (5 min), pSTAT5

(**IV**) STAT3 knock-down, OSM+VEGF (5 min), pERK

(**V**) STAT3 knock-down, OSM+VEGF (30 min, 1 h), pSTAT1

(**VI**) STAT3 knock-down, OSM+VEGF (6 h, 24 h), pSTAT1

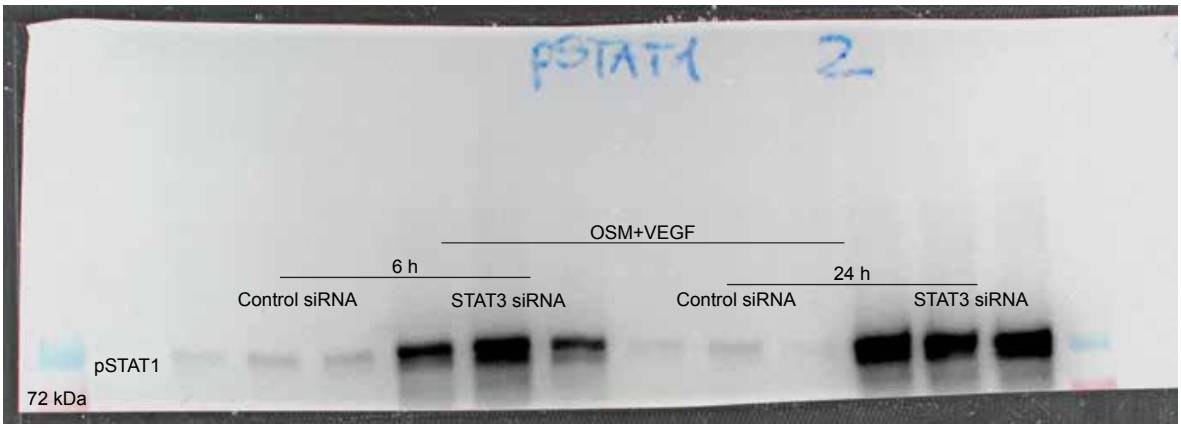

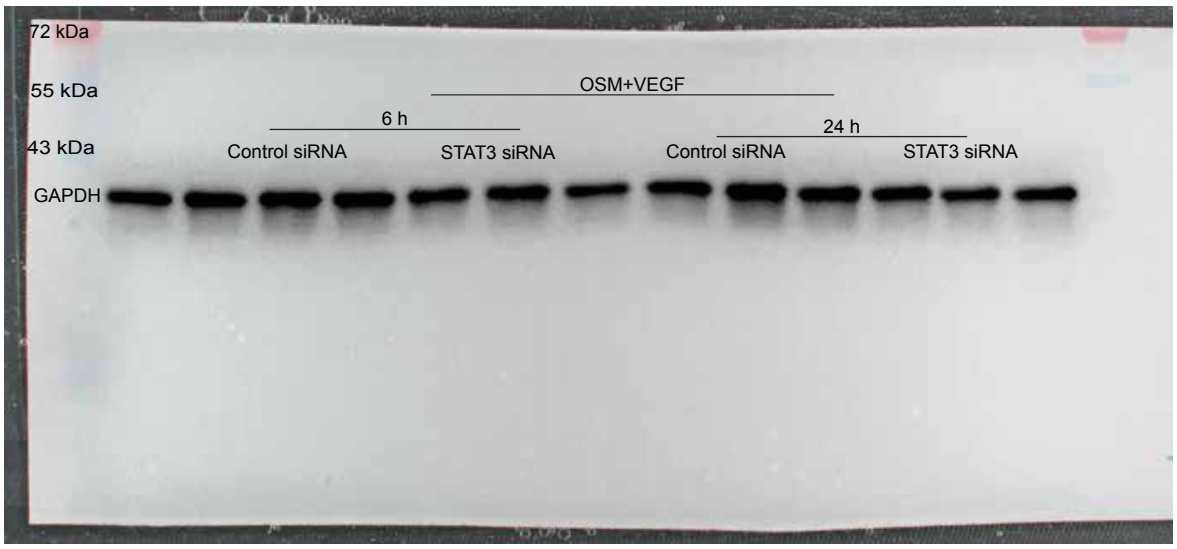

Fig. S10.

(**I**) Mitochondrial complexes 1

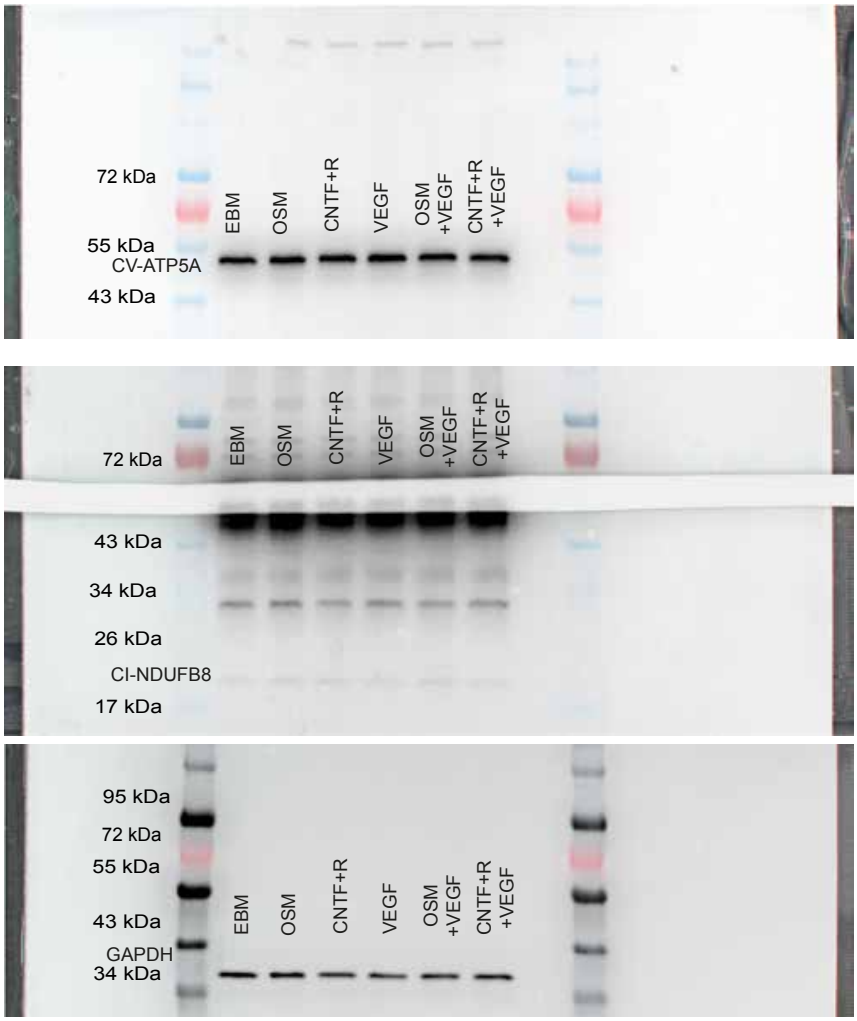

(**II**) Mitochondrial complexes 2

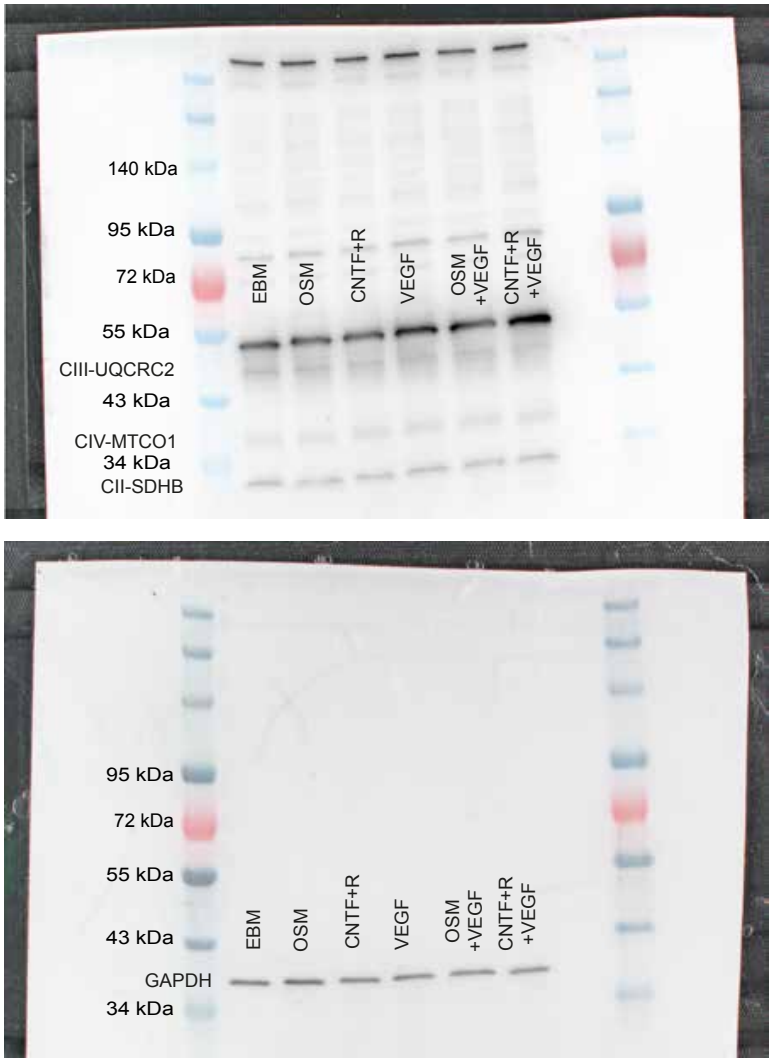

Fig. S11.

(**I**) pJAK1, no co-stimulation with VEGF

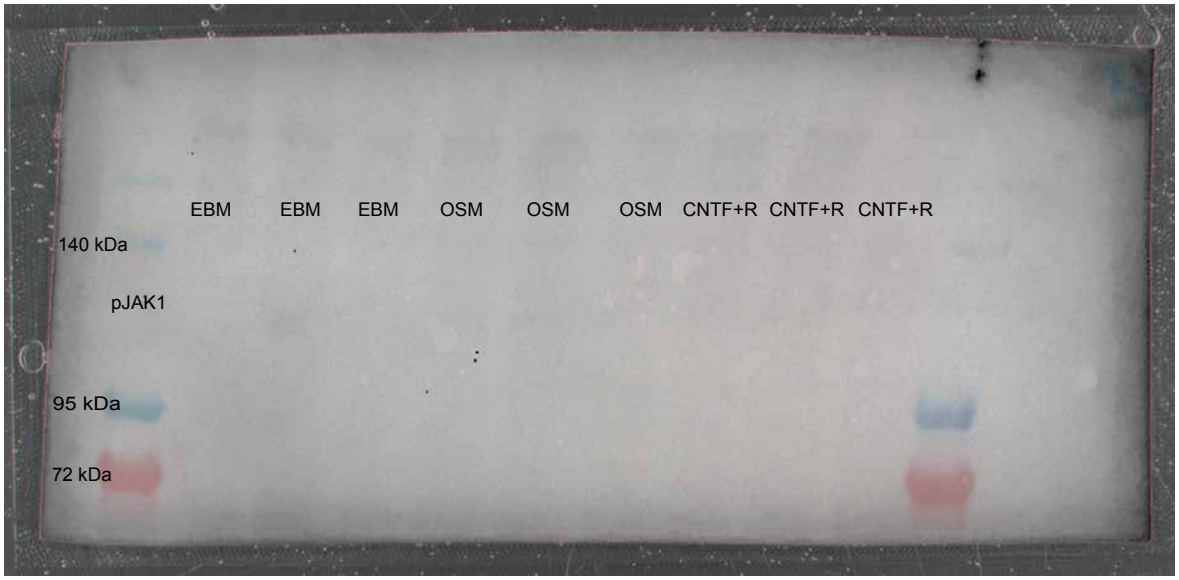

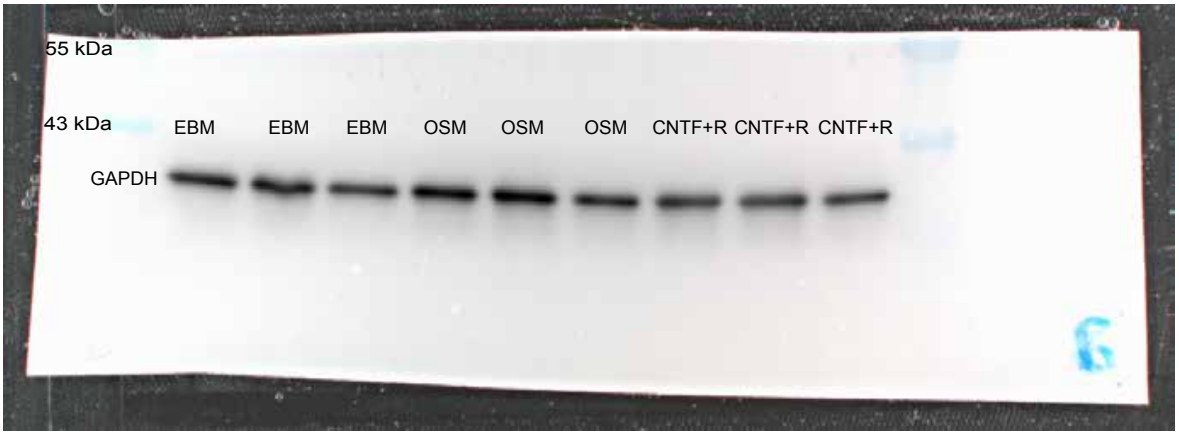

(**II**) pJAK2, no co-stimulation with VEGF

(**III**) pTYK2, no co-stimulation with VEGF

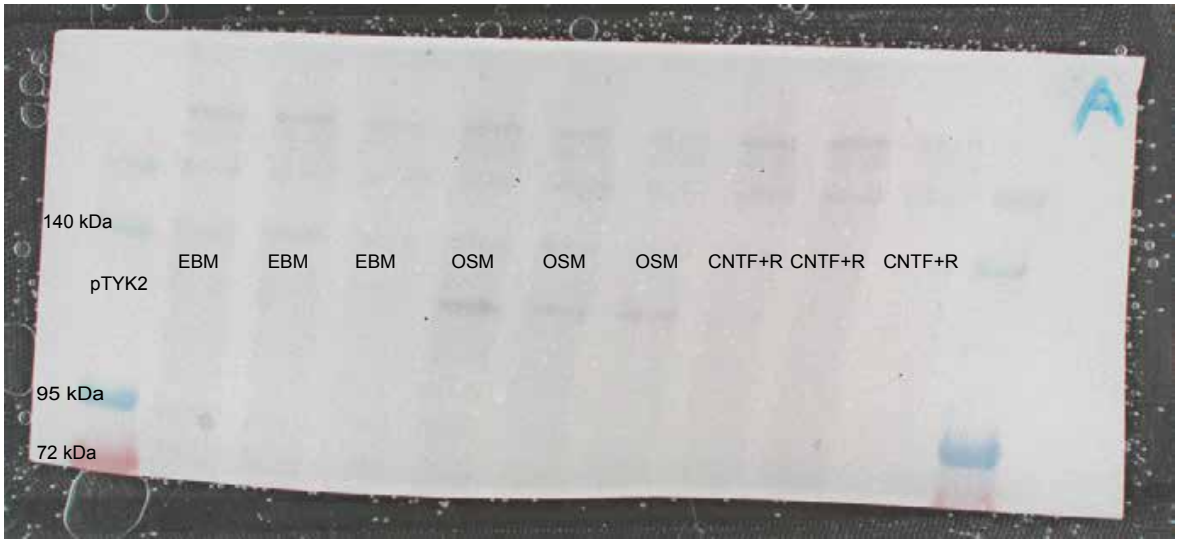

(**IV**) pJAK1, co-stimulation with VEGF

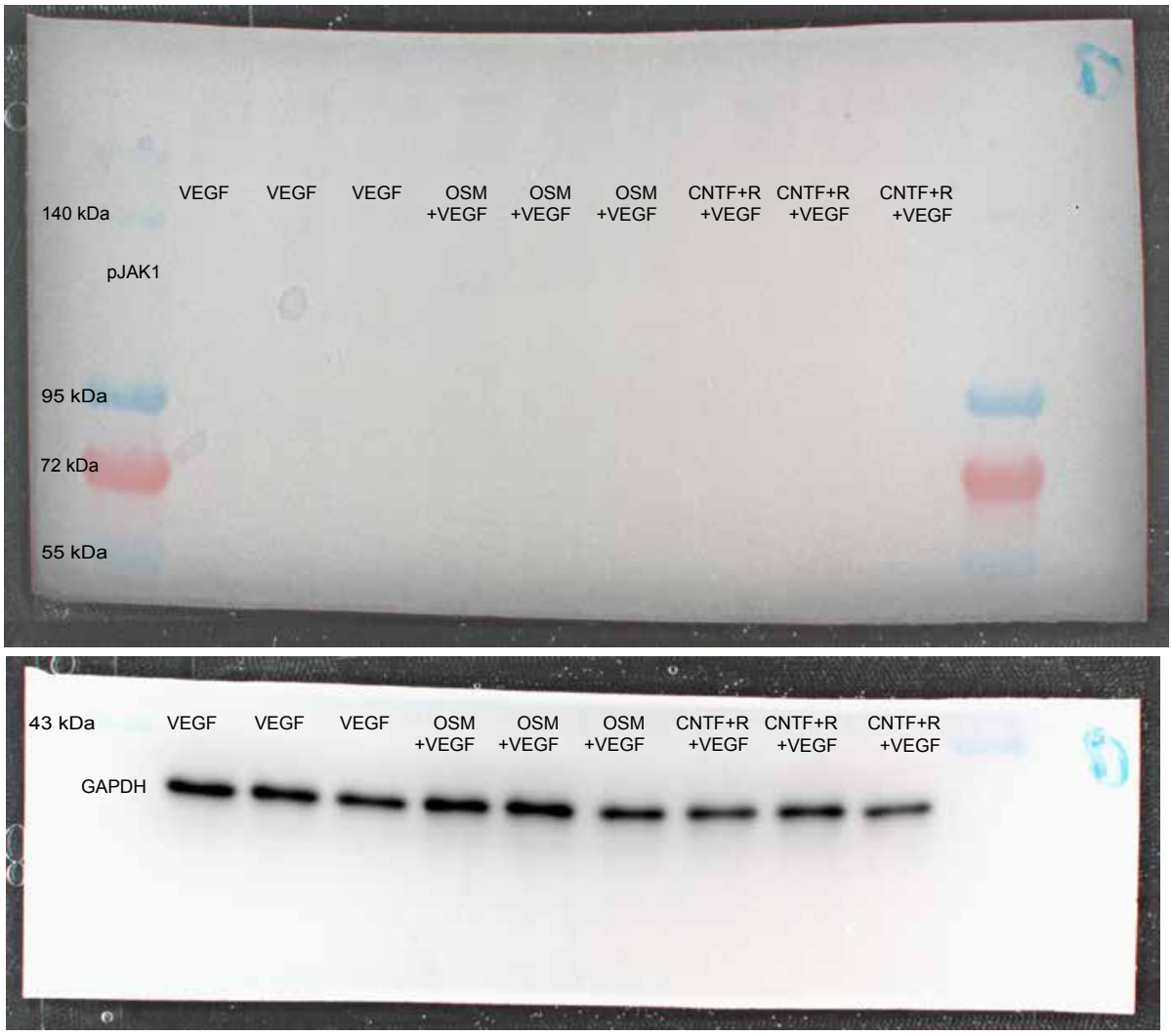

(**V**) pJAK2, co-stimulation with VEGF

(**VI**) pTYK2, co-stimulation with VEGF

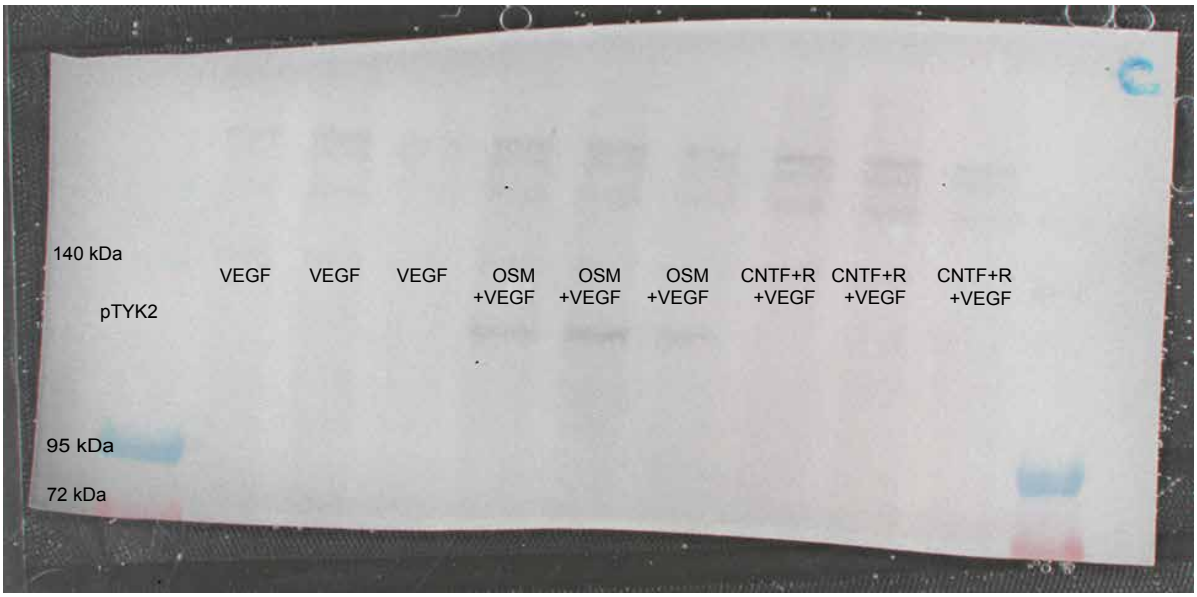

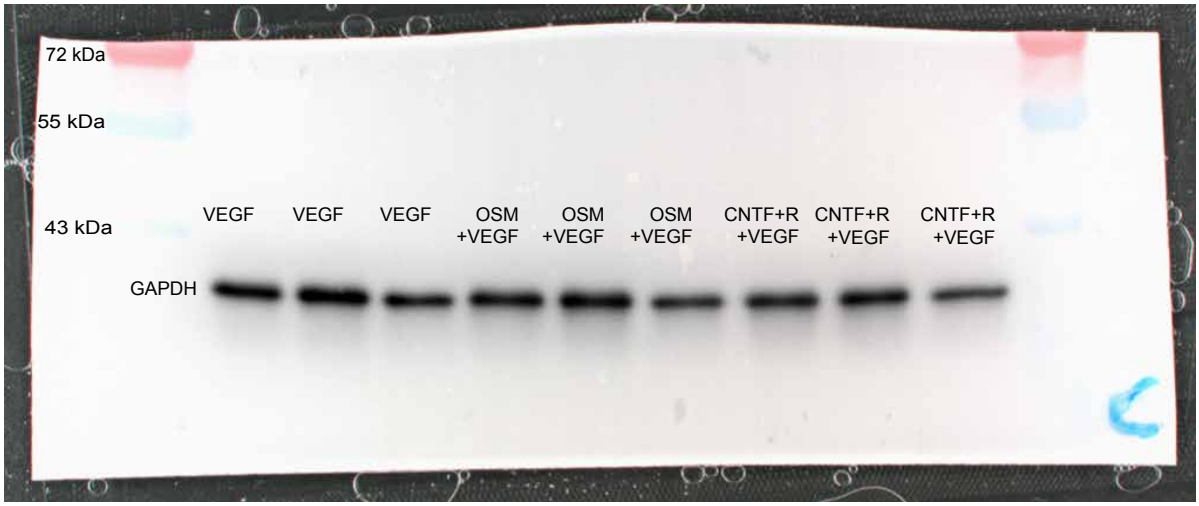

(**VII**) OSM kinetics (1)

(**VIII**) OSM kinetics (2)

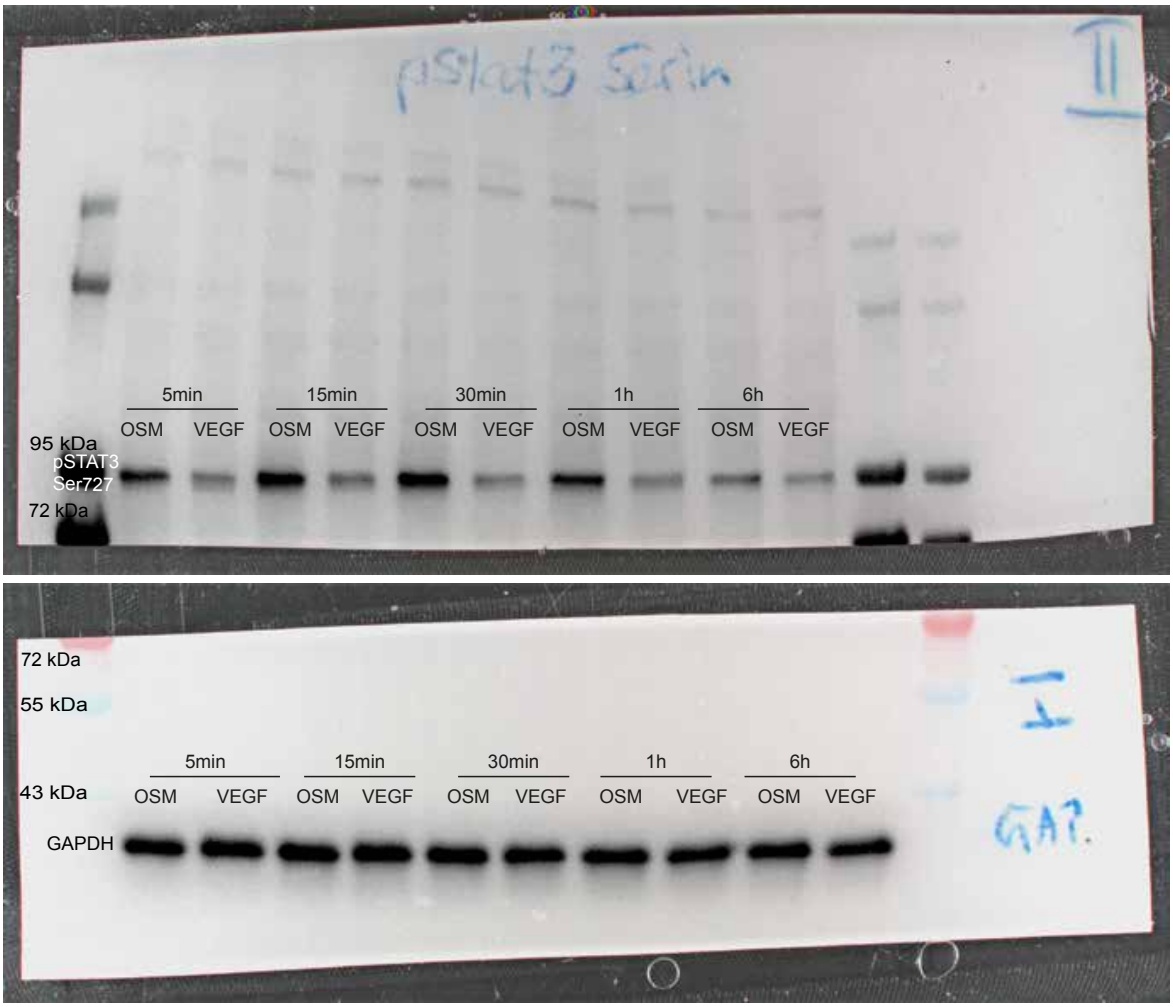

(**XI**) CNTF+R kinetics

Fig. S12.

(**I**) STAT3 knock-down, siRNA 1

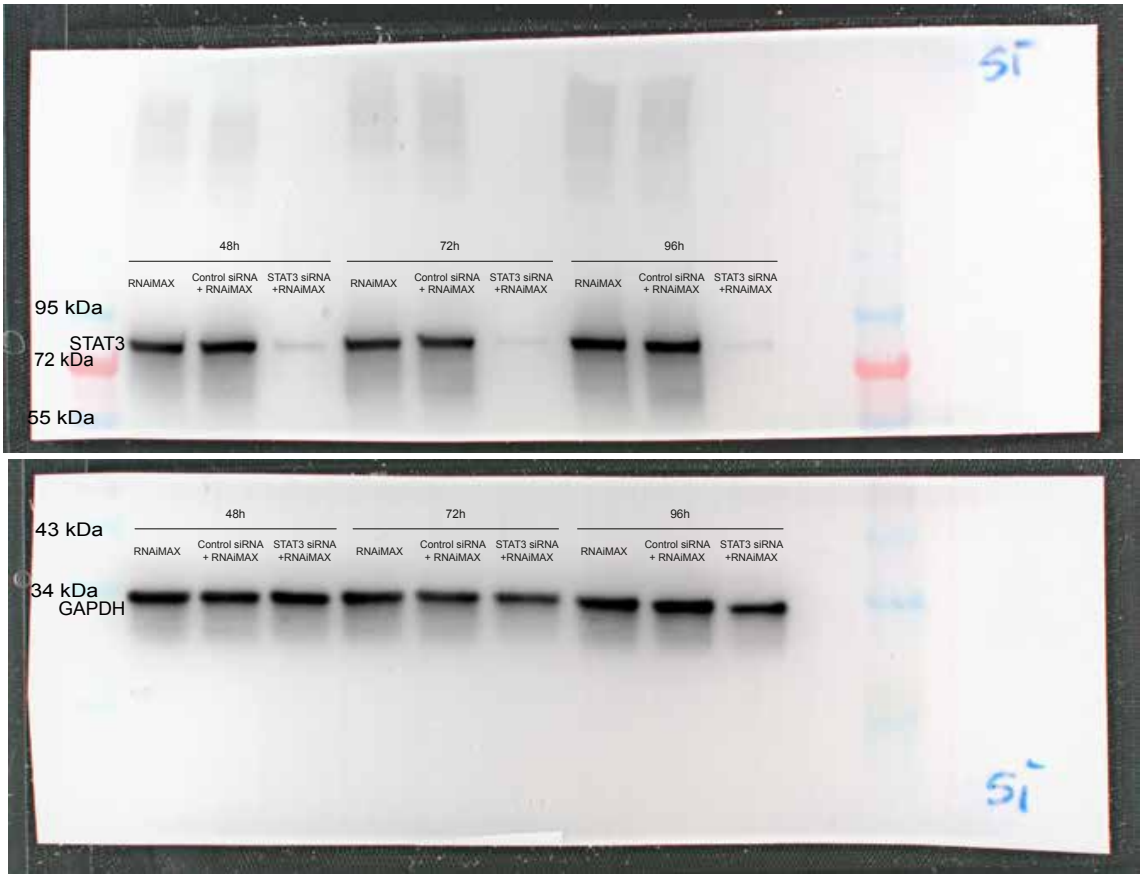

(**II**) STAT3 knock-down, siRNA 2

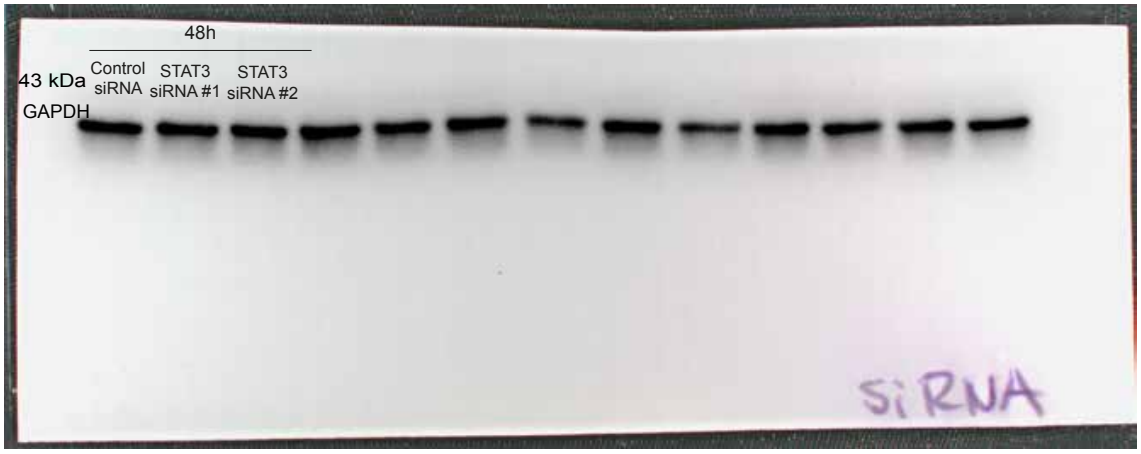

(**III**) STAT1 knock-down

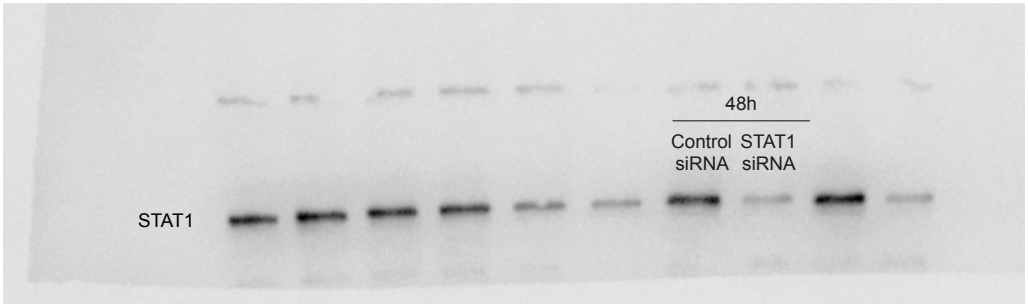

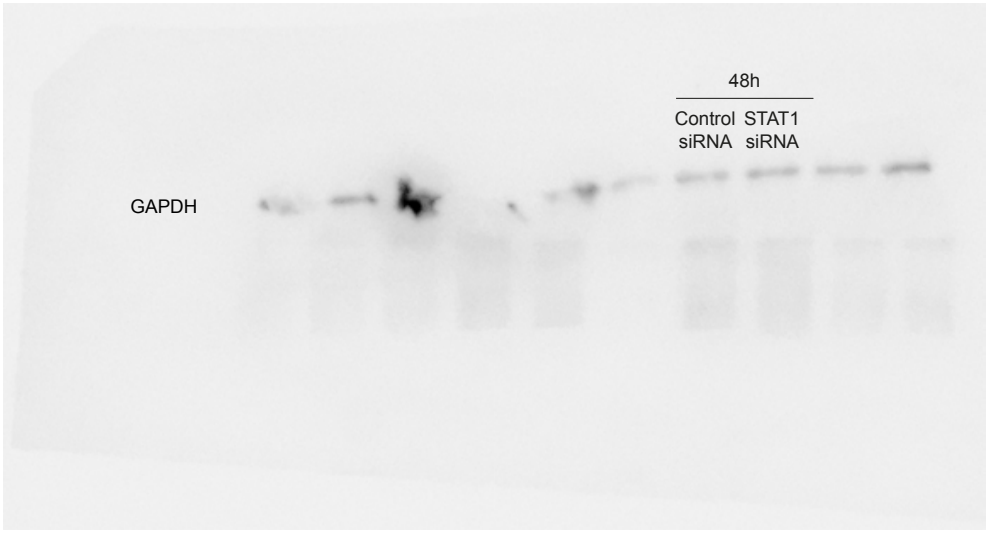

Table S1. Cytokines used.

Cytokine	Source	Cat#:	Final Concentration
OSM	Peprotech	300-10	100 ng/mL
CNTF	Peprotech	450-13	100 ng/mL
CNTFR	R&D Systems	303-CR	200 ng/mL
VEGF	Peprotech	100-20	25 ng/mL

Table S2. Antibodies used.

Antigen	Source	Cat#:	Final Concentration
pSTAT3 (Tyr705)	Cell Signaling	9145	1:2000
pSTAT3 Ser(727)	Cell Signaling	9134	1:1000
pSTAT1	Cell Signaling	9167	1:1000
pSTAT5	Cell Signaling	9359	1:1000
pAKT	Cell Signaling	4060	1:2000
pERK	Cell Signaling	4370	1:2000
pJAK1	Cell Signaling	74129	1:1000
pJAK2	Cell Signaling	8082	1: 1000
pTYK2	Cell Signaling	68790	1:1000
STAT3	Cell Signaling	4904	1:2000
OxPhos Rodent WB Antibody Cocktail	Thermo Fisher	45-8099	1:250
GAPDH	Merck	MAB374	1:10000
Goat Anti Rabbid	Jackson	111-035-003	1:10000

Table S3. Top 10 GO Terms (Biological processes) with their specific ID and the corresponding number of DEGs annotated to those terms in the RNA sequencing analysis between OSM+VEGF vs CNTF+R+VEGF stimulated HUVECs which enriched for OSM+VEGF.

GO Term	ID	# of DEGs	Total Number
inflamatory response	GO:0006954	17	788
response to cytokine	GO:0034097	17	1113
regulation of cellular component movement	GO:0051270	15	12006
enzyme linked receptor protein signaling pathway	GO:0007167	15	1002
cytokine-mediated signaling pathway	GO:0019221	14	438
regulation of cell migration	GO:0030334	14	1010
extracellular matrix organization	GO:0030198	9	323
extracellular structure organization	GO:0043062	9	324
bone resorption	GO:0045453	5	80
regulation of IL1-mediated signaling pathway	GO:2000659	3	7

Table S4. GO Terms (Molecular function) with their specific ID and the corresponding number of DEGs annotated to those terms in the RNA sequencing analysis between OSM+VEGF vs CNTF+R+VEGF stimulated HUVECs which enriched for OSM+VEGF.

GO Term	ID	# of DEGs	Total Number
cytokine receptor binding	GO:0005126	8	321
growth factor binding	GO:0019838	7	146
cytokine activity	GO:0005125	7	232
growth factor receptor binding	GO:0070851	5	151
cytokine binding	GO:0019955	5	147
insulin-like growth facter I binding	GO:0005520	3	18
plated-derived growth factor receptor binding	GO:0005161	3	14
insulin-like growth factor binding	GO:0005520	3	18

Table S5. Top 15 GO Terms (Biological processes) with their specific ID and the corresponding number of DEGs annotated to those terms in the RNA sequencing analysis between OSM+VEGF stimulated HUVECs with or without STAT3 knock-down which enriched for the knock-down group.

GO Term	ID	# of DEGs	Total Number
regulation of cell adhesion	GO:0030155	57	826
regulation of protein kinase activty	GO:0045859	56	614
regulation of MAPK cascade	GO:0043408	55	752
response to virus	GO:0009615	50	367
positive regulation of MAPK cascade	GO:0043410	45	540
positive reg. of cell migration	GO:0030335	43	596
circulatory system process	GO:0003013	42	579
defense response to virus	GO:0051607	40	305
leukocyte proliferation	GO:0070661	34	395
response to interferon-gamma	GO:0034341	30	148
cellular response to interferon-gamma	GO:0071346	29	119
type I interferone signaling pathway	GO:0060337	23	58
cellular response to type I interferon	GO:0071357	23	58
response to type I interferon	GO:0034340	23	64
leukocyte homeostasis	GO:0001776	15	137

Table S6. Top 15 GO Terms (Biological processes) with their specific ID and the corresponding number of DEGs annotated to those terms in the RNA sequencing analysis between OSM+VEGF stimulated HUVECs with or without STAT3 knock-down which enriched for the control siRNA group.

GO Term	ID	# of DEGs	Total Number
monocarboxylic acid metablic process	GO:0032787	60	674
regulation of secretion by cell	GO:1903530	58	703
extracellular matrix organization	GO:0030198	52	323
extracellular structure organization	GO:0043062	52	324
cell-cell adhesion via plasmamembrane adhesion molecules	GO:0098742	34	218
negative regulation of growth	GO:0045926	30	267
homophilic cell adhesion via plasma membrane adhesion	GO:0007156	25	114
nicotinamide nucleotide biosynthetic process	GO:0019359	10	16

pyridine nucleotide biosynthetic process	GO:0019363	10	19
	GO:0019362	10	71
nicotinamide nucleotide metabolic process	GO:0046496	10	69
pyridine-containing compound biosynthetic process	GO:0072525	10	23
pyridine-containing compound metabolic process	GO:0072524	10	80
NAD biosynthetic process	GO:0009435	9	12
detoxification of copper ion	GO:0010273	6	6

Table S7. Top 15 GO Terms (Biological processes) with their specific ID and the corresponding number of DEGs annotated to those terms in the RNA sequencing analysis between CNTF+R+VEGF stimulated HUVECs with or without STAT3 knock-down which enriched for the knock-down group.

GO Term	ID	# of DEGs	Total Number
response to virus	GO:0009615	31	367
defense response to virus	GO:0051607	26	305
response to interferon-gamma	GO:0034341	26	148
cellular response to interferone-gamme	GO:0071346	24	119
type I interferon signaling pathway	GO:0060337	22	58
response to molecule of bacterial origin	GO:0002237	20	411
cellular response to type I interferon	GO:0071357	22	58
response to lipopolysaccharide	GO:0032496	19	390
response to type I interferon	GO:0034340	22	64

interferon-gamma-mediated signaling pathway	GO:0060333	16	25
negative regulation of viral process	GO:0048525	11	112
neutrophil chemotaxis	GO:0030593	10	104
negative regulation of viral genome replication	GO:0045071	9	67
defense response to protozoan	GO:0042832	6	39
response to protozoan	GO:0001562	6	44

Table S8. Top 15 GO Terms (Biological processes) with their specific ID and the corresponding number of DEGs annotated to those terms in the RNA sequencing analysis between CNTF+R+VEGF stimulated HUVECs with or without STAT3 knock-down which enriched for the control siRNA group

GO Term	ID	# of DEGs	Total Number
cell−cell adhesion via plasmamembrane adhesion molecules	GO:0098742	27	218
carboxylic acid biosynthetic process	GO:0046394	24	307
organic acid biosynthetic process	GO:0016053	24	310

extracellular matrix organization	GO:0030198	24	323
extracellular structure organization	GO:0043062	24	324
homophilic cell adhesion via plasma membrane adhesion molecules	GO:0007156	21	114
regulation of cell morphogenesis involved in differentiation	GO:0010769	23	130
developmental growth involved in morphogenesis	GO:0060560	18	288
developmental cell growth	GO:0048588	18	284
neuron projection extension	GO:1990138	16	208
regulation of axonogenesis	GO:0050770	16	187
leukocyte tethering or rolling	GO:0050901	7	38
regulation of leukocyte tethering or rolling	GO:1903236	5	22
neurotransmitter receptor transport to plasma membrane	GO:0098877	5	23
neurotransmitter receptor transport to	GO:0098969	5	21
postsynaptic membrane			

Table S9. Top 15 GO Terms (Biological processes) with their specific ID and the corresponding number of DEGs annotated to those terms in the RNA sequencing analysis between VEGF stimulated HUVECs with or without STAT3 knock-down which enriched for the control siRNA group

GO Term	ID	# of DEGs	Total Number
extracellular matrix organization	GO:0030198	20	323
extracellular structure organization	GO:0043062	20	324

Table S10. GO Terms (Biological processes) with their specific ID and the corresponding number of DEGs annotated to those terms in the RNA sequencing analysis between VEGF stimulated HUVECs with or without STAT3 knock-down which enriched for the control siRNA group

GO Term	ID	# of DEGs	Total Number
small molecule biosynthetic process	GO:0044283	35	564
carboxylic acid biosynthetic process	GO:0046394	24	307
organic acid biosynthetic process	GO:0016053	24	310
monocarboxylic acid biosynthetic process	GO:0072330	18	215